CrossMark

J. Fluid Mech. (2016), *vol.* 808, *pp.* 116–152. © Cambridge University Press 2016. This is a work of the U.S. Government and is not subject to copyright protection in the United States.
doi:10.1017/jfm.2016.540

Compressibility effects in the shear layer over a rectangular cavity

Steven J. Beresh[1,†], **Justin L. Wagner**[1] **and Katya M. Casper**[1]

[1]Sandia National Laboratories, Albuquerque, NM 87185, USA

(Received 30 March 2016; revised 26 June 2016; accepted 10 August 2016; first published online 26 October 2016)

The influence of compressibility on the shear layer over a rectangular cavity of variable width has been studied in a free stream Mach number range of 0.6–2.5 using particle image velocimetry data in the streamwise centre plane. As the Mach number increases, the vertical component of the turbulence intensity diminishes modestly in the widest cavity, but the two narrower cavities show a more substantial drop in all three components as well as the turbulent shear stress. This contrasts with canonical free shear layers, which show significant reductions in only the vertical component and the turbulent shear stress due to compressibility. The vorticity thickness of the cavity shear layer grows rapidly as it initially develops, then transitions to a slower growth rate once its instability saturates. When normalized by their estimated incompressible values, the growth rates prior to saturation display the classic compressibility effect of suppression as the convective Mach number rises, in excellent agreement with comparable free shear layer data. The specific trend of the reduction in growth rate due to compressibility is modified by the cavity width.

Key words: compressible turbulence, high-speed flow, shear layer turbulence

1. Introduction

Among the many applications of cavity flows are aircraft weapons bays. Given the wide range of speeds over which aircraft fly, the effects of increasing compressibility are relevant in the prediction of flow over cavities and the resulting resonant loading on aircraft structures or carried stores. Compressibility in cavities also becomes pertinent when considering airframe gaps or recessed projectile features that are a prime source of drag, whose properties change with Mach number. The progressing use of cavities as scramjet flameholders also raises the issue of compressible alterations to models of the cavity flow physics derived from studies at lower speeds.

When the cavity is reasonably short, less than a length-to-depth ratio L/D of approximately 6–8 in subsonic flows (Tracy & Plentovich 1997) and approximately 10 in supersonic flows (Stallings & Wilcox 1987), the flow is considered to be ‘open’. A feedback loop is established between the shear layer impinging upon the rear of the cavity and the aeroacoustic field confined within the cavity walls.

† Email address for correspondence: sjberes@sandia.gov

https://doi.org/10.1017/jfm.2016.540 Published online by Cambridge University Press

This produces longitudinal resonance tones of narrow frequency character and considerable amplitude.

The frequencies of these resonances, but not their amplitudes, are well predicted in simple cavity geometries by a semi-empirical equation attributed to Rossiter (1964), although in practice most engineers use the modified form by Heller & Bliss (1975) that improves the compressibility term. This equation offers a simple method of identifying the resonance frequencies to which a store in the cavity would be subjected, but it masks the complex physics that occurs in a cavity flow and affects the aeroacoustic environment. In particular, the Rossiter equation is dependent upon constants representing the convection velocity within the cavity and the phase delay in upstream wave propagation, both of which later were found to be functions of the Mach number (Clark, Kaufman & Maciulaitus 1980; Malone *et al.* 2009). As the Mach number becomes significantly supersonic, the physics of cavity resonance appears to shift towards a different acoustic model and agreement with the Rossiter equation may be merely fortuitous (Zhang & Edwards 1990; Murray & Elliott 2001; Unalmis, Clemens & Dolling 2004). Still, many decades of use has shown that the Rossiter equation does a reasonable job of predicting the resonance frequencies of a simple rectangular cavity even if it is not based on sound physics.

Few previous studies have examined the effects of compressibility on cavity flow structure, although many have been concerned with the variations in aeroacoustic properties with Mach number. Krishnamurty (1955) likely provided the first measurements of the Mach dependence of cavity resonance tones and their acoustic radiation. Many subsequent wind tunnel tests systematically measured the resonance tones in cavities of varied dimensions to examine the acoustic environment as a function of Mach number (e.g. Plumblee, Gibson & Lassiter 1962; Ahuja & Mendoza 1995; Tracy & Plentovich 1997) and support the continued use of Heller and Bliss's version of the Rossiter equation to reasonably predict the tonal frequencies across a wide range of Mach numbers.

Aside from schlieren imaging of waves emanating from cavities, studies of the variation of cavity flow structure with Mach number awaited improved measurement technology, and yet remain uncommon. Murray & Elliott (2001) covered a range of supersonic Mach numbers using planar laser scattering to examine large-scale turbulent structures in the shear layer over a two-dimensional cavity, determining that as the Mach number rises, the structure size decreases and becomes less coherent. They further suggested that this trend, while similar to that found in free shear layers, is not as strong in cavity flows. Murray, Sallstrom & Ukeiley (2009) used particle image velocimetry (PIV) to measure the shear layer and recirculation region for several subsonic and transonic Mach numbers. Their data show the shifting position of the recirculation region as the Mach number changes and also indicate a rise in the turbulence intensity with increased Mach number. Although the vast literature of cavity flows covers a thorough range of Mach numbers, no other known studies have examined the cavity flow field structure while varying the Mach number.

Conversely, the effects of compressibility on the turbulence of free shear layers have been well studied. In fact, the subject has received such attention that multiple reviews of it may be found (Lele 1994; Dutton 1997; Smits & Dussauge 2006). Aside from its practical application, the study of compressibility in free shear layers is attractive because such effects become prominent at considerably lower Mach numbers than for wall-bounded flows. The degree of compressibility in shear layers can be defined by the convective Mach number, which first was conceived by Bogdanoff (1983) and then established in its presently accepted form by Papamoschou & Roshko (1988).

https://doi.org/10.1017/jfm.2016.540 Published online by Cambridge University Press

The convective Mach number is defined as $M_c = (U_1 - U_2)/(a_1 + a_2)$ when both fluid streams are composed of the same gas. Here, U is the free stream velocity and a is the speed of sound, with subscripts 1 and 2 denoting the high-speed and low-speed streams, respectively.

A compilation of numerous experiments shows that as M_c rises, turbulence is suppressed within the shear layer, which has a number of important ramifications. Most widely observed is a reduction in the growth rate of the shear layer in comparison with its incompressible counterpart and hence a thinner shear layer at equivalent downstream distance (e.g. Papamoschou & Roshko 1988; Hall, Dimotakis & Rosemann 1993; Clemens & Mungal 1995; Rossmann, Mungal & Hanson 2002). At the same time, the large-scale turbulent structures seen to dominate the incompressible shear layer gradually become smaller, less organized, and more three-dimensional (e.g. Samimy, Reeder & Elliott 1992; Hall *et al.* 1993; Clemens & Mungal 1995). Visualizations of the turbulent structure show that the behaviour of the shear layer alters once M_c increases past approximately 0.6, at which point the dominant instability shifts from the Kelvin–Helmholtz instability to an oblique instability (Clemens & Mungal 1995; Elliott, Samimy & Arnette 1995). Simulations support this observation (Sandham & Reynolds 1991).

Velocimetry data of compressible shear layers are rarer, but particularly relevant to understanding the effects of increasing compressibility on turbulence. Laser Doppler velocimetry measurements by Goebel & Dutton (1991) showed that the transverse (vertical, in the terms of the present article) component of the turbulence intensity and the turbulent shear stress are considerably reduced with increasing M_c but the streamwise turbulence intensity is minimally reduced, if at all. Gruber, Messersmith & Dutton (1993) confirmed these trends and added that the spanwise component remains fairly constant. Similar measurements by Elliott & Samimy (1990) concurred regarding the transverse turbulence intensity and the turbulent shear stress, but found that the streamwise component of the turbulence intensity diminishes as well. The simulations of Freund, Lele & Moin (2000) agree with Goebel and Dutton. Additional velocimetry experiments by Barre, Quine & Dussauge (1994) and Debisschop, Chambres & Bonnet (1994) appear to support this view as well but contain ambiguities. Finally, PIV data by Urban & Mungal (2001) and Olsen & Dutton (2003) are consistent with the Goebel and Dutton viewpoint.

Though studies of compressible effects on turbulence in free shear layers are plentiful, this is not the case for cavity flows. The limited attention to compressibility in the cavity shear layer is unfortunate, as there are several reasons why the shear layer behaviour over a cavity can be expected to differ from a free shear layer. Most evidently, in free shear layers, both free streams are considered uniform and constant, but in a cavity, the slower free stream is actually the boundary of the recirculation region, thereby inducing a boundary condition that varies spatially and temporally. The Kelvin–Helmholtz instabilities that drive the unsteady free shear layer behaviour may be continually excited by the distinct acoustic tones present in cavity resonance (Gharib & Roshko 1987; Rowley, Colonius & Basu 2002). Furthermore, impingement of the shear layer on the aft cavity wall is known to affect the shear layer position and therefore change the upstream influence (Rockwell & Knisely 1979; Liu & Katz 2013). Given these contrasts, it is unclear whether the compressibility effects so evident in free shear layers will be reproduced in cavity shear layers in a similar fashion or may exhibit differing behaviour.

Moreover, cavity flows are subject to geometric influences not present in free shear layers. One of these is the nature of two- versus three-dimensional cavity

https://doi.org/10.1017/jfm.2016.540 Published online by Cambridge University Press

flows, which previously has been explored by the present authors (Beresh *et al.* 2015*a*,*b*). For simplicity of imaging diagnostics, many cavity experiments utilize a two-dimensional configuration, in which the cavity extends across the entire wind tunnel test section with windows at either side. Although this provides easy optical access into the depths of the cavity, it alters the nature of both the flow field and the acoustics by neglecting effects of a three-dimensional cavity – that is, one of finite width. In the latter configuration, spillage of external fluid falls into the cavity over the two side lips and forms streamwise-aligned vortices that would not occur in a two-dimensional arrangement (Dudley & Ukeiley 2011; Crook, Lau & Kelso 2013; Ohmichi & Suzuki 2014). The very presence of the cavity side walls creates spanwise instabilities (Maull & East 1963; Rockwell & Knisely 1980; Larchevêque, Sagaut & Labbé 2007; Brès & Colonius 2008; Faure *et al.* 2009; Basley *et al.* 2013) and these have been found to modulate the amplitude of the resonances in a manner that varies with the cavity width (Ahuja & Mendoza 1995; Tracy & Plentovich 1997; Disimile, Toy & Savory 2000; Chung 2001; Zhang & Naguib 2011).

Such behaviour also may have precedent in free shear layers, whose turbulent structure is influenced by the presence of side walls (Zhuang, Dimotakis & Kubota 1990; Morris & Giridharan 1991; Clemens & Mungal 1992). It is reasonable to infer from this that the cavity walls similarly may alter the turbulence in the shear layer. The spacing between these walls – that is, the cavity width – may not only change the flow field structure, as shown by Beresh *et al.* (2015*a*,*b*), but also may affect the degree to which compressibility has an effect on the shear layer growth and inhibition of turbulence.

The existing PIV data sets of Beresh *et al.* (2015*a*,*b*) span a free stream Mach number range of 0.6–2.5. As calculated later in the present article, this corresponds to an estimated convective Mach number reaching 1.01. Cavity length-to-depth ratio was fixed at 5 while the length-to-width ratio varied from 1 to 5. These data offer an opportunity to explore the influence of compressibility on the turbulence properties of the cavity shear layer and compare the results to those known for free shear layers. Although (Beresh *et al.* 2015*a*) previously discussed compressibility effects on the cavity shear layer, these were examined in limited detail and only for supersonic conditions. Therefore, the present article revisits the two earlier data sets with the specific interest of analysing the compressibility effects.

2. Experimental methods

2.1. *Wind tunnel and cavity hardware*

Experiments were performed in Sandia's Trisonic Wind Tunnel (TWT), which is a blowdown-to-atmosphere facility using air as the test gas through a test section enclosed within a pressurized plenum. In its transonic configuration, the test section is a straightforward rectangular duct of dimensions 305 mm $\times$ 305 mm with interchangeable walls. Porous walls ordinarily are used for testing near sonic conditions when blockage relief is needed and solid walls are used when imaging diagnostics require windows. For the present experiments, the test section was configured with porous walls on the top wall and one side wall to alleviate non-physical resonances due to wind tunnel duct modes (Wagner *et al.* 2015*a*); a solid wall with a window for imaging was installed in the other side of the test section. Despite the non-uniform test section, no evidence of flow asymmetry was detected in either pressure or PIV data.

Supersonic experiments were conducted in the TWT's half-nozzle test section, in which the top wall of each supersonic nozzle is retained and a single lower wall

https://doi.org/10.1017/jfm.2016.540 Published online by Cambridge University Press

extends the inlet contour of the tunnel before fairing into a flat surface at what previously would have been the test section centreline. This provides a flat plate working surface with convenient optical access within the 'test rhombus' in which the supersonic expansion is complete, as opposed to the full test section that requires sting-mounted models for testing. The resulting half-nozzle test section is 152 mm high and 305 mm wide.

In the present study, transonic experiments were conducted at Mach numbers 0.60, 0.80 and 0.94, and supersonic experiments were conducted at Mach numbers 1.5, 2.0 and 2.5. Transonic flow conditions were selected to hold the free stream dynamic pressure q_∞ constant at 33 kPa. The supersonic data, on the other hand, were acquired using stagnation pressures designed to achieve a common Reynolds number based on the incoming boundary layer thickness of approximately 400 000, compared to approximately 200 000 for the transonic cases. Supersonic values of q_∞ were much higher, between 110 and 133 kPa. Previous PIV measurements and Pitot probe surveys have shown that the incoming 99 %-velocity boundary layer thickness ranges from approximately 10–15 mm for the entire Mach range of the present experiments, which is 40 %–60 % of the cavity depth (see below). Since the boundary layer thickness remains within the same range for all cases and the change in Reynolds number is relatively small for a fully turbulent flow, the difference in flow conditions is not expected to be evident in normalized data. Indeed, no effect has been found on the normalized unsteady pressures (Zhuang *et al.* 2003; Gai, Kleine & Neely 2015; Wagner *et al.* 2015*b*), nor does it significantly alter the velocity field or turbulent stresses (based on supplementary data collected as part of the Beresh *et al.* (2015*a*) experiment).

The wind tunnel stagnation temperature T_0 is fixed at 321 K $\pm$ 2 K by heating in the storage tanks, and the wall temperature is effectively constant at ambient conditions, $T_w = 307$ K $\pm$ 3 K. Free stream velocities U_∞ were measured from previous PIV experiments as 215, 280, 315, 450, 535 and 605 m s^{-1} for the six cases in order of increasing Mach number, estimated to be accurate to within 0.3 %.

The finite-width cavity of the present experiments is simply a rectangular pocket in a plate inserted into the lower test section wall, as shown in figure 1. The cavity geometry is identical for both the supersonic and the transonic configurations, although its streamwise position within the test section varies mildly. The floor of the cavity is a BK7 glass flat to allow the laser sheet for the PIV measurements to enter the test section from below. The cavity has dimensions 127 mm $\times$ 127 mm (5 in. $\times$ 5 in.) with a nominal depth of 25.4 mm (1 in.). In practice, the cavity depth was measured to be 25.9 mm (1.02 in.) for the supersonic configuration but achieved the intended dimension of 25.4 mm for the transonic experiments, due to a discrepancy in the crush of a gasket. In addition to the widest cavity dimensions of 127 mm $\times$ 127 mm, insert blocks can be bolted against the cavity side walls to reduce the cavity width for additional tests. This was used to create cavities of 127 mm $\times$ 76 mm (5 in. $\times$ 3 in.) and 127 mm $\times$ 25 mm (5 in. $\times$ 1 in.); the cavity depth was not changed. The respective length-to-width ratios L/W are 1.00, 1.67 and 5.00; the length-to-depth ratio L/D is 4.90 for the three supersonic conditions and 5.00 for the three transonic conditions. These three cavity configurations henceforth will be denoted the 5 $\times$ 5, the 5 $\times$ 3 and the 5 $\times$ 1 cases. The coordinate system was chosen such that x lies in the streamwise direction and y is vertical, positive away from the cavity, with the z coordinate spanwise and right handed. The origin is the spanwise centre of the cavity leading edge.

https://doi.org/10.1017/jfm.2016.540 Published online by Cambridge University Press

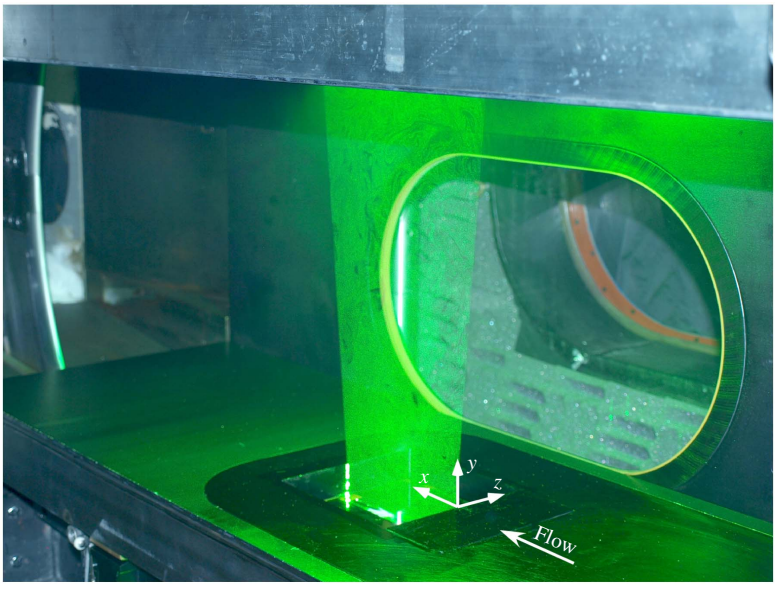


FIGURE 1. (Colour online) The 127×127 mm^2 (5×5 in.^{2}) cavity installed into the floor of the transonic test section with the PIV laser sheet.

2.2. *High-frequency pressure sensors*

Dynamic pressure measurements were made at multiple locations along the fore and aft walls of the cavity using piezoresistive sensors (Kulite XCQ-062-50A or equivalent) whose frequency response is flat to approximately 50 kHz. This exceeds the frequency of the highest detectable cavity resonance tones by nearly an order of magnitude. In the present case, data are shown only from a sensor placed at the spanwise centre of the cavity aft wall, which is representative of the aeroacoustic environment throughout the cavity. The sensors were powered by a voltage amplifier (Endevco Model 136) that also amplified the resulting pressure signals and passed them to a low-pass filter (Krohn-Hite Model 3384) with a cutoff frequency of 50 kHz. Data were digitized at 14 bits and 200 kHz (National Instruments PXI 6133). The measurement capability is described in more detail in Wagner *et al.* (2015*b*) although a slightly different cavity geometry was tested.

Pressure data are shown as power spectra computed using Welch's periodogram method, Blackman windows, a 50 % overlap between data segments and a frequency resolution of 10 Hz. Spectral amplitudes are given normalized by dynamic pressure and the repeatability has been shown to be within 0.5 % of full scale.

2.3. *Particle image velocimetry*

Two data sets have been collected, both described previously (Beresh *et al.* 2015*a*,*b*). Despite any inference based on publication dates, the supersonic measurements were collected several years prior to the transonic measurements and were somewhat less mature.

In PIV experiments, the TWT is seeded by a thermal smoke generator using a mineral oil base (Corona Vi-Count 5000) whose output has been previously measured *in situ* by tracking the particle response across a shock wave to show a particle size

https://doi.org/10.1017/jfm.2016.540 Published online by Cambridge University Press

of 0.7–0.8 μm. Stokes numbers have been estimated as at most 0.05 based on *a posteriori* measurements of typical cavity shear layer eddies, which is sufficiently small to render particle lag errors negligible. Inspection of PIV images of the recirculation region in the cavity shows that, although the particle density drops at the highest Mach numbers, sufficient particles are retained for high vector quality in all regions.

2.3.1. *Supersonic measurements*

The supersonic experiment was itself composed of two distinct measurement campaigns. A two-component configuration surveyed the entire streamwise extent of the cavity by peering partially into the cavity at an angle. This provided the best spatial coverage possible using only two cameras, but the viewing angle introduced an uncorrectable perspective bias error in the vertical velocity component and still could not reach the cavity floor. Conversely, a stereoscopic configuration provided more accurate data using the same two cameras in a smaller field of view covering approximately the downstream half of the cavity. Steeper camera angles reached the cavity floor without introducing perspective error owing to the stereoscopic calibration and availability of three components of velocity.

In either configuration, the light source for the PIV system was a frequency-doubled dual cavity Nd:YAG laser (Spectra Physics PIV-400) that produced 300–400 mJ per beam. The beams were formed into coplanar sheets and directed into the test section from beneath the wind tunnel, then entered the cavity through the window forming its floor. The laser sheet thickness was 1.0 mm and was aligned to the spanwise centre of the cavity. The time between laser pulses varied between 0.5 and 1.5 μs depending on measurement configuration and free stream velocity and was chosen to avoid out-of-plane particle dropout while maintaining 10–15 pixels of in-plane displacement at free stream velocities.

Scattered laser light was collected by interline-transfer charge-coupled device (CCD) cameras (LaVision Imager ProX 4MP) with a resolution of 2048 × 2048 pixels digitized at 14 bits. The two cameras were equipped with 105 mm lenses for the two-component PIV and 200 mm lenses for the stereoscopic PIV; in both cases, the lenses were mounted on Scheimpflug platforms to align an oblique focal plane with the laser sheet. For the two-component configuration, the cameras were placed side by side to survey an extent of the cavity twice as large in the streamwise dimension as in the vertical dimension. The cameras peered down into the cavity at an angle of 11°, and an alignment target placed at the laser sheet location was used to produce a calibration that could account for the variable magnification due to the viewing angle.

For stereoscopic data, the cameras viewed the imaging region using compound angles and two-axis Scheimpflug focusing, where half-angles of 12° separated the two cameras in the streamwise plane and both were angled identically in the vertical plane at 38° to look into the cavity. The 12° streamwise half-angle is sub-optimal for stereoscopic measurements, but a greater angle would have suffered occlusion of the field of view by the trailing edge of the cavity. Stereoscopic camera calibrations were accomplished by placing a single-plane alignment target in the position of the laser sheet, then scanning it through the volume of the laser sheet to acquire seven planes of calibration data, which were calibrated using a polynomial fit.

Data were processed using LaVision's DaVis v7.2. Image pairs were interrogated with an initial pass using 64 × 64 pixel interrogation windows, followed by two iterations of 32 × 32 pixel interrogation windows, which translates into a spatial

https://doi.org/10.1017/jfm.2016.540 Published online by Cambridge University Press

resolution of approximately 0.8 mm per vector for both measurement configurations. A 50 % overlap in the interrogation windows was used as well. The resulting vector fields were validated based upon signal-to-noise ratio, nearest-neighbour comparisons and allowable velocity range. For all data shown herein, at least 750 vector fields were acquired for each experimental case combining Mach number and cavity width.

2.3.2. *Transonic measurements*

By the time the transonic experiment was conducted, four cameras were available to survey the entire streamwise extent of the cavity using two stereoscopic fields of view. The same laser was used and configured identically, save that the sheet thickness was 1.5 mm and time between laser pulses was between 0.9 and 1.3 μs.

The four cameras (all LaVision sCMOS, each with a resolution of 2560 × 2160 pixels digitized at 16 bits) were equipped with 200 mm lenses mounted on Scheimpflug platforms viewing the imaging region using compound angles. As in the supersonic experiment, half-angles of 12° separated the two cameras of each stereo pair in the streamwise plane and the cameras were tilted in the vertical plane at approximately 35° to provide sufficient angle to view the cavity floor. Stereoscopic camera calibrations were performed identically to the supersonic measurements and self-calibration was used to minimize camera registration error. Data processing was as the supersonic experiment but used DaVis 8.2. Approximately 3000 vector fields were acquired for each case.

2.3.3. *Uncertainty quantification*

Measurement uncertainty in the PIV data was treated in some depth in Beresh *et al.* (2015*a*) for the supersonic experiments and need not be repeated here in its entirety. The earlier approach was modified for the present analysis to focus on turbulence quantities. The random uncertainty of each independent measurement was estimated from the standard deviation of PIV measurements in the free stream, which must bound the true error as they are a combination of measurement error and free stream turbulence. Bias errors, principally resulting from the stereoscopic calibration, were examined by Beresh *et al.* (2015*a*) and found to have a considerable effect on mean velocities but only a small effect on turbulence quantities. This occurs because biases are of low spatial frequency and largely cancel out when velocity fluctuations are computed. In the present uncertainty quantification, calibration biases are neglected without significant alteration of the uncertainty estimates.

The uncertainty of turbulent stresses has been estimated by incorporating both convergence uncertainty and precision error of the constituent velocity fluctuations. The fractional convergence uncertainty of a standard deviation is found simply from $1/\sqrt{(2N-1)}$, where N is the number of vector fields (Taylor 1997). Precision uncertainties in each component of the turbulent stress and the vorticity thickness (see § 5) were propagated from the random uncertainty using a Taylor expansion, then added to the convergence uncertainty in a root-sum-square fashion. Rather than calculating uncertainties for each point in the flow, uncertainties were conservatively estimated by considering only the most turbulent region of the cavity, centred in the shear layer near the aft end of the cavity. For Mach 0.8, this yielded typical uncertainties of 0.007, 0.009 and 0.011 on the u, v and w components of the turbulence intensities, respectively, and 0.002 for the $u'v'$ turbulent shear stress (non-dimensionalized by the free stream velocity). Uncertainty was estimated independently at Mach 0.8 and Mach 2 to represent the transonic and supersonic experiments, but in practice the resulting uncertainty bands were very similar.

https://doi.org/10.1017/jfm.2016.540 Published online by Cambridge University Press

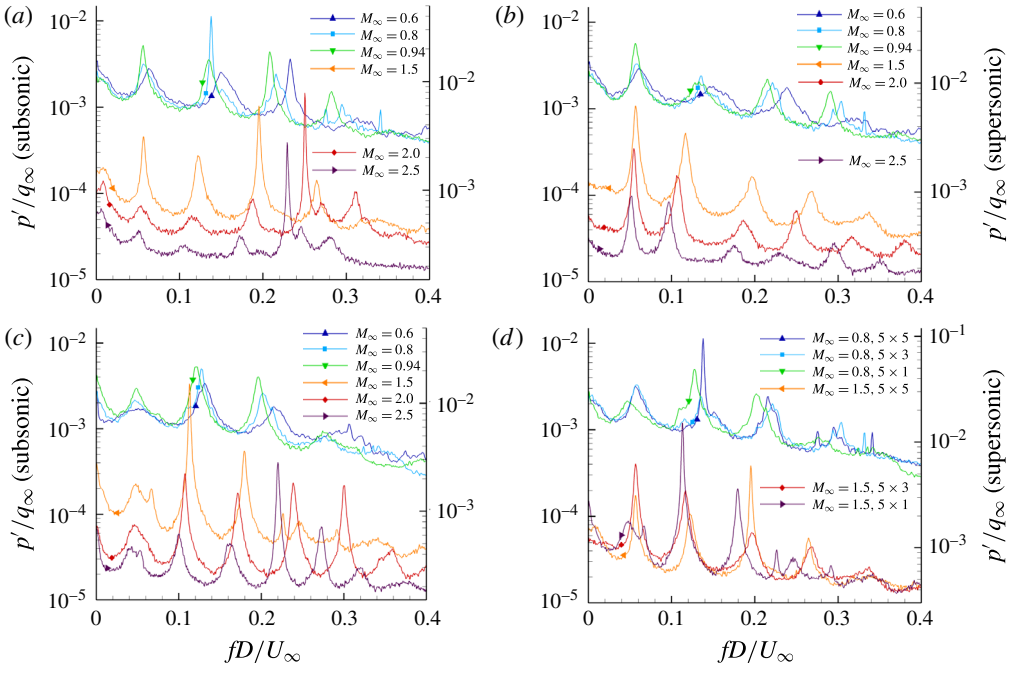


FIGURE 2. (Colour online) Pressure power spectra for all cavity widths and Mach numbers. Subsonic and supersonic cases are shown on separate y axes. (*a*) 5 × 5 cavity; (*b*) 5 × 3; (*c*) 5 × 1; (*d*) all cavity widths at Mach 0.8 and 1.5 only.

3. Acoustic fields

As noted in the introduction, Mach number effects on cavity acoustics have long been known and discussed. Fluctuating pressure measurements similar to the present flow have been discussed at length for all Mach numbers by Wagner *et al.* (2015*b*) although only for a single, related cavity geometry. Pressure data are briefly described here to establish the resonance conditions found in the cavity. Hydrodynamic effects are present in the pressure data, but the resonance peaks that dominate the spectra are acoustic phenomena.

Figure 2 provides the pressure power spectra for the three cavity widths at all Mach numbers, with pressure fluctuation amplitude shown normalized by the free stream dynamic pressure to remove any influence of the wind tunnel stagnation pressure. The subsonic and supersonic cases are shown on different y axes to separate the curves for clarity. If plotted coincidentally, the baseline intensity of the three subsonic spectra resides at values noticeably greater than those of the Mach 1.5 case, with a slight trend of decreasing intensity as the Mach number is raised from 0.6 to 0.94.

In all cases, there is a general trend in which the non-dimensional frequency (Strouhal number) of each resonance tone decreases as the Mach number is raised, in accordance with the Rossiter equation. This effect becomes stronger at higher frequencies and is evident despite changes in the resonance magnitudes, which do not appear to follow a predictable trend. Also as the Mach number increases, the magnitude of the background acoustic intensity diminishes, which is only weakly evident for the subsonic data but obvious for the supersonic cases. A few peaks are observed to split (e.g. Mach 0.8 for the 5 × 5 cavity at $fD/U_\infty = 0.28$; Mach 1.5

https://doi.org/10.1017/jfm.2016.540 Published online by Cambridge University Press

for the 5 × 1 cavity at $fD/U_\infty = 0.06$), but since these are found for supersonic conditions as well as subsonic, it implies that they are not necessarily a residual effect of wind tunnel wall interference (Wagner *et al.* 2015*a*). None of these trends appear to be influenced by the cavity width.

To examine effects of the cavity width upon the acoustic field, figure 2(*d*) replots the data at Mach 0.8 and 1.5 for all three geometries. The tone frequencies of the 5 × 5 and 5 × 3 cavities are usually very close, but the 5 × 1 cavity typically displays lower tone frequencies. This may be a consequence of the absence (or great reduction) of side-wall spillage for the narrow 5 × 1 configuration in contrast with the two wider cavities (Beresh *et al.* 2015*a*,*b*; Arunajatesan *et al.* 2014). Tone amplitude also is seen to be a function of the cavity width.

4. Velocity and turbulence fields

4.1. *Mean velocity field*

A representative mean velocity field of the cavity flow is shown in figure 3. This is the case of the 5 × 5 cavity at Mach 0.8, which is well measured by the dual stereoscopic PIV system and broadly indicative of the flow for all cases. The white box drawn in figure 3 shows the more limited field of view of the supersonic stereoscopic measurements in subsequent figures. The vector field captures the shear layer over the top of the cavity, its impingement on the aft wall and the recirculation of flow near the floor of the cavity. Mean reverse velocities reach approximately $-0.25U_\infty$. The recirculation region is seen to dominate the cavity flow field and extend over nearly its entire streamwise length. As noted in Beresh *et al.* (2015*a*), the general flow structure along the streamwise centre plane of the cavity strongly resembles similar measurements both incompressible and subsonic compressible (e.g. Zhuang *et al.* 2006; Haigermoser *et al.* 2008; Murray *et al.* 2009) even though such experiments were conducted in a two-dimensional cavity whereas the present study uses a finite-width geometry.

4.2. *Streamwise turbulence intensity*

Figure 4 shows the streamwise turbulence intensity of the cavity for the 5 × 5 case and four of the six Mach numbers. Superposed on these contours are streamlines derived from the mean velocity field to identify the overall flow field structure. Mach 0.8 represents the three subsonic cases, since the non-dimensional flow field was found to not change significantly from Mach 0.6 to Mach 0.94. The Mach 0.8 plot is formed from the dual stereoscopic measurements, but the three supersonic plots are composites of the two-dimensional field of view and the stereoscopic field of view. Combining them in this manner expands the coverage of the cavity from the available measurements. This approach is useful only for the streamwise velocity component as the vertical component is biased for the two-dimensional measurements and of course the spanwise component is absent.

The fundamental structure of the cavity flow is invariant with Mach number for the u' fields in figure 4. The size and position of the mean recirculation region does not appear to change appreciably, although closer inspection suggests that it shrinks in size slightly as the Mach number rises with the reduction in length isolated to its upstream extent. The thickness of the shear layer based on u' is constant with Mach number. The peak magnitudes of the streamwise turbulence intensity also remain constant within the shear layer, although at Mach 2.5 the magnitudes are

https://doi.org/10.1017/jfm.2016.540 Published online by Cambridge University Press

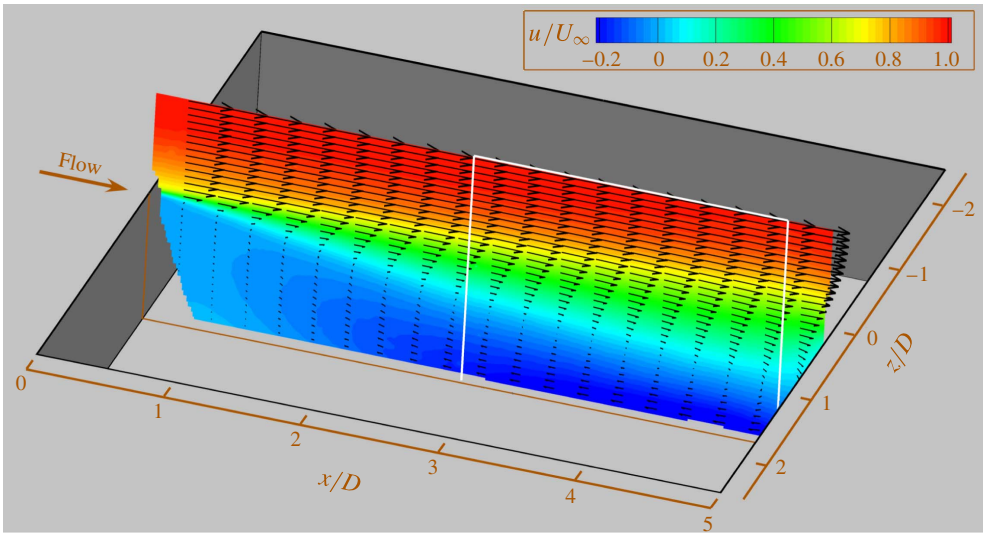


FIGURE 3. (Colour online) Mean velocity field for the 5 × 5 cavity at Mach 0.8, which is representative of the general flow structure for all cases. The white box shows the field of view of the supersonic stereoscopic measurements in subsequent figures.

lowered somewhat very near the cavity floor where reverse velocities will be greatest. Therefore, at most, compressibility induces only minor changes to the flow field of the 5 × 5 cavity when the streamwise component of turbulence intensity is considered.

Analogous plots are shown in figure 5 for the 5 × 3 cavity. Here, a composite plot is available only for the Mach 1.5 case, as two-component data were not acquired more generally because of the more limited depth to which the measurement could reach for this geometry. Instead, solely the stereoscopic field of view is shown for Mach 2 and Mach 2.5.

A comparison to figure 4 can establish how the cavity width influences the flow field structure. First, unlike the 5 × 5 configuration, the Mach number influences the shear layer and recirculation region in the 5 × 3 cavity. The supersonic cases suggest that the recirculation region has a greater upstream extent than the Mach 0.8 case, although the depiction of the streamlines may be influenced by the more limited field of view. For all Mach numbers, the 5 × 3 cavity has a recirculation region situated nearer the cavity floor than the 5 × 5 cavity, which is the principal difference in the mean flow field between these two cavity widths. In addition, the subsonic cases show a recirculation region more limited in extent for the 5 × 3 cavity than the 5 × 5 (Beresh *et al.* 2015*b*) with an aft position within the cavity. In supersonic conditions it is longer and shifted farther upstream (Beresh *et al.* 2015*a*), and it displays a noticeable aftward movement for the two highest Mach numbers, which did not occur for the 5 × 5 cavity.

Contrary to the 5 × 5 cavity, the shear layer in the 5 × 3 cavity appears to thin with rising Mach number in figure 5. At the same time, the magnitude of u' diminishes in both the shear layer and the recirculation region, which is in contrast to the 5 × 5 cavity. These trends constitute compressibility effects on the flow field, and their presence is dependent upon the cavity width.

https://doi.org/10.1017/jfm.2016.540 Published online by Cambridge University Press

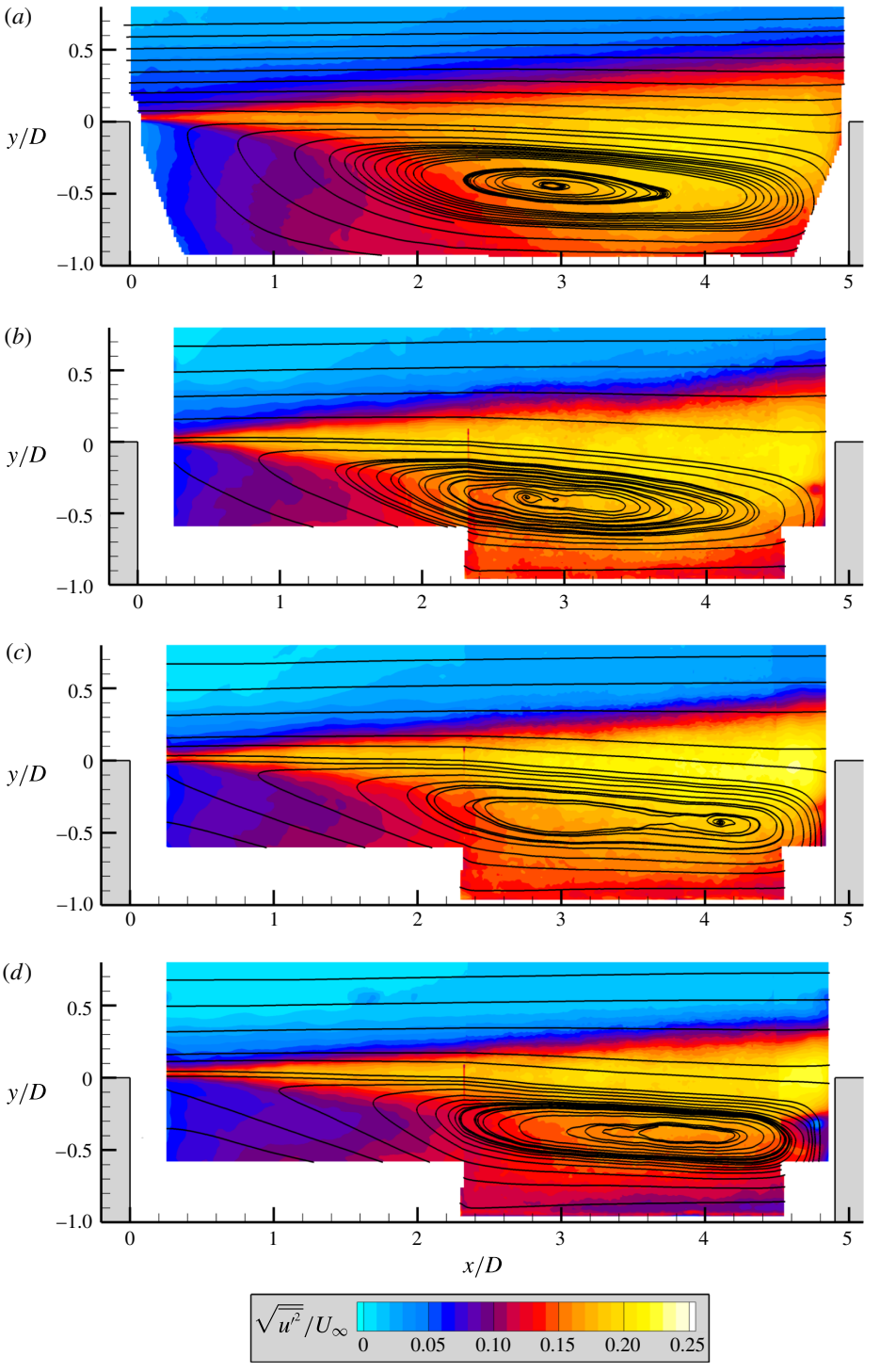


FIGURE 4. (Colour online) Streamwise turbulence intensity fields for the 5 × 5 cavity with superposed streamlines derived from the mean velocity field; (*a*) Mach 0.8; (*b*) Mach 1.5; (*c*) Mach 2; (*d*) Mach 2.5.

https://doi.org/10.1017/jfm.2016.540 Published online by Cambridge University Press

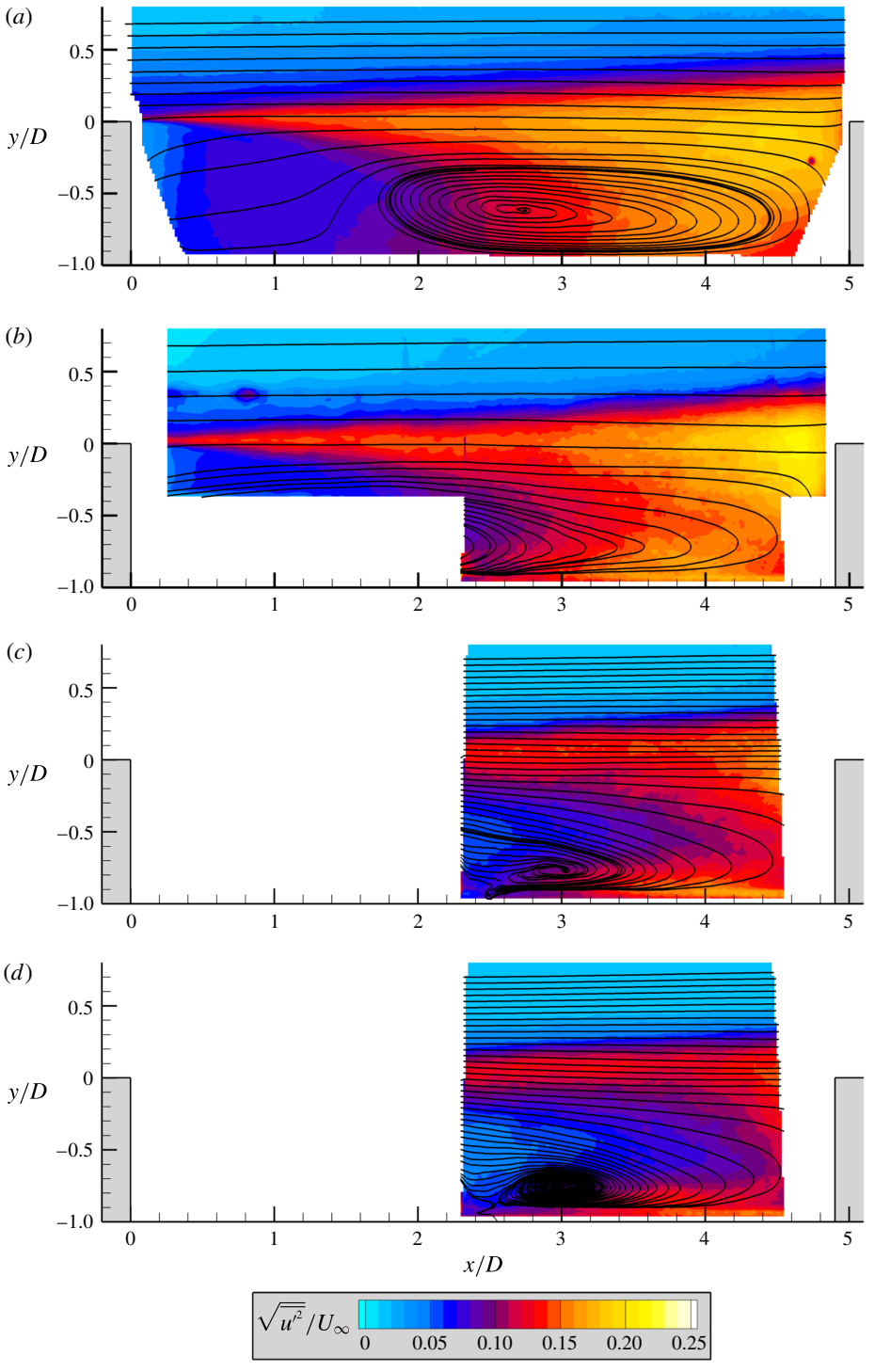


FIGURE 5. (Colour online) As figure 4, but for the 5 × 3 cavity.

https://doi.org/10.1017/jfm.2016.540 Published online by Cambridge University Press

The shear layer is difficult to observe for the 5 × 1 cavity due to the limited visibility into the cavity, and the recirculation region cannot be seen at all. Just enough of the shear layer can be viewed to suggest that it may thin at Mach 2 and 2.5 and that u' diminishes a small but significant degree. For brevity, these plots are omitted due to the reduced spatial coverage, but they will be shown subsequently for the vertical component of the turbulence intensity where the results are more conclusive within the limited field of view.

The present turbulence data may be compared to several previous investigations that have reported similar measurements in a cavity, though flow conditions and geometry differ. The most nearly matched to the present configuration is the work described in Ukeiley & Murray (2005) and Murray *et al.* (2009), which report a maximum streamwise turbulence intensity in the cavity shear layer of 0.25 at Mach 0.2, in reasonable agreement with the present value of 0.22 at Mach 0.8 in the 5 × 5 cavity. Similar measurements have been made in incompressible cavity flows of other L/D ratios, yielding streamwise turbulence intensities from 0.13 to 0.23 (Grace, Dewar & Wroblewski 2004; Haigermoser *et al.* 2008; Basley *et al.* 2011). All these experiments studied a two-dimensional cavity, and as the present measurements have shown, the width of the cavity affects the turbulence levels on the centreline. Therefore, the range of peak turbulence values is not unexpected and in agreement with the present work as well as can be considered plausible.

4.3. *Vertical turbulence intensity*

Some difference in behaviour can be observed in the 5 × 5 cavity where the vertical component of the turbulence intensity is concerned, shown in figure 6. The magnitudes of v' are lower than those of u', which is readily evident since both are plotted on the same contour scale. The maximum measured value is 0.16, in excellent agreement with the Mach 0.73 data of Murray *et al.* (2009) and consistent with two other incompressible experiments (Haigermoser *et al.* 2008; Basley *et al.* 2011). As the Mach number rises, v' falls distinctly in the shear layer. This is in contrast to u' in figure 4, in which the shear layer did not display a reduction as the Mach number was increased. The v' component also diminishes with Mach number in the recirculation region, which for u' was only marginally observable at Mach 2.5.

Figure 7 shows that the magnitudes of v' are lower for the 5 × 3 cavity than the 5 × 5 cavity, which previously has been noted (Beresh *et al.* 2015*a*,*b*). For this cavity width, the compressibility effect on v' is even more striking. Intensity magnitudes fall further with increasing Mach number than they did for the 5 × 5 cavity and the shear layer extent based on v' is notably thinner as well. Turbulence magnitudes also drop sharply within the recirculation region at higher Mach numbers.

Data from the 5 × 1 cavity are shown for v' in figure 8 despite the limited measurement penetration into the depths of the cavity. The intensity magnitude of this component of turbulence is similar to the 5 × 5 cavity at Mach 0.8. At Mach 1.5, the intensity magnitude rises slightly, which also was observed for u' (but not shown in a figure). Then, as the Mach number increases to 2 and 2.5, v' drops markedly, whereas it displayed only a small decrease in u'. At these two highest Mach numbers, the shear layer thins sufficiently that its bottom edge becomes visible even within the limited field of view. No comment on the influence of compressibility on the recirculation region is possible.

https://doi.org/10.1017/jfm.2016.540 Published online by Cambridge University Press

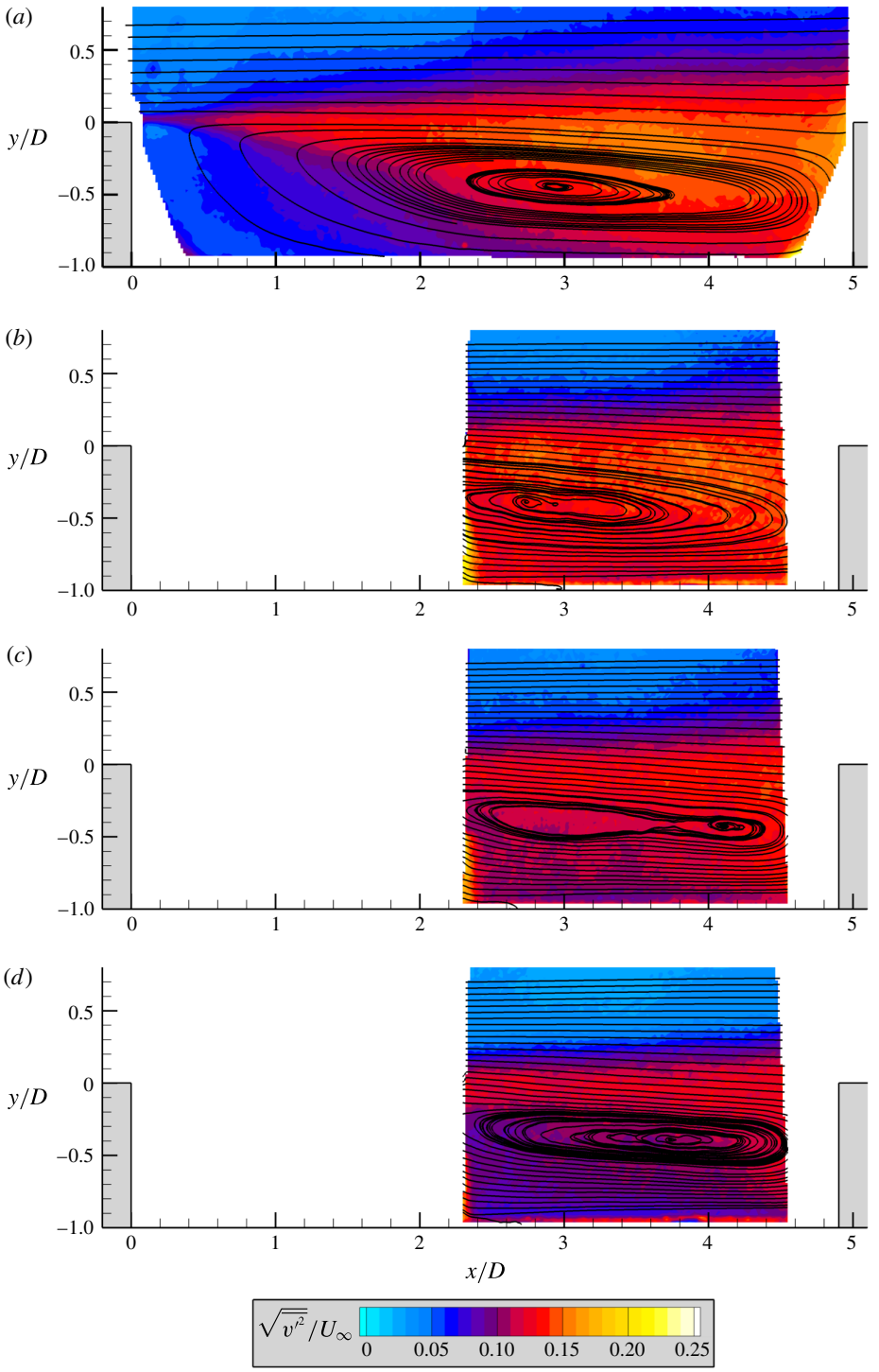


FIGURE 6. (Colour online) Vertical turbulence intensity fields for the 5 × 5 cavity with superposed streamlines derived from the mean velocity field; (*a*) Mach 0.8; (*b*) Mach 1.5; (*c*) Mach 2; (*d*) Mach 2.5.

https://doi.org/10.1017/jfm.2016.540 Published online by Cambridge University Press

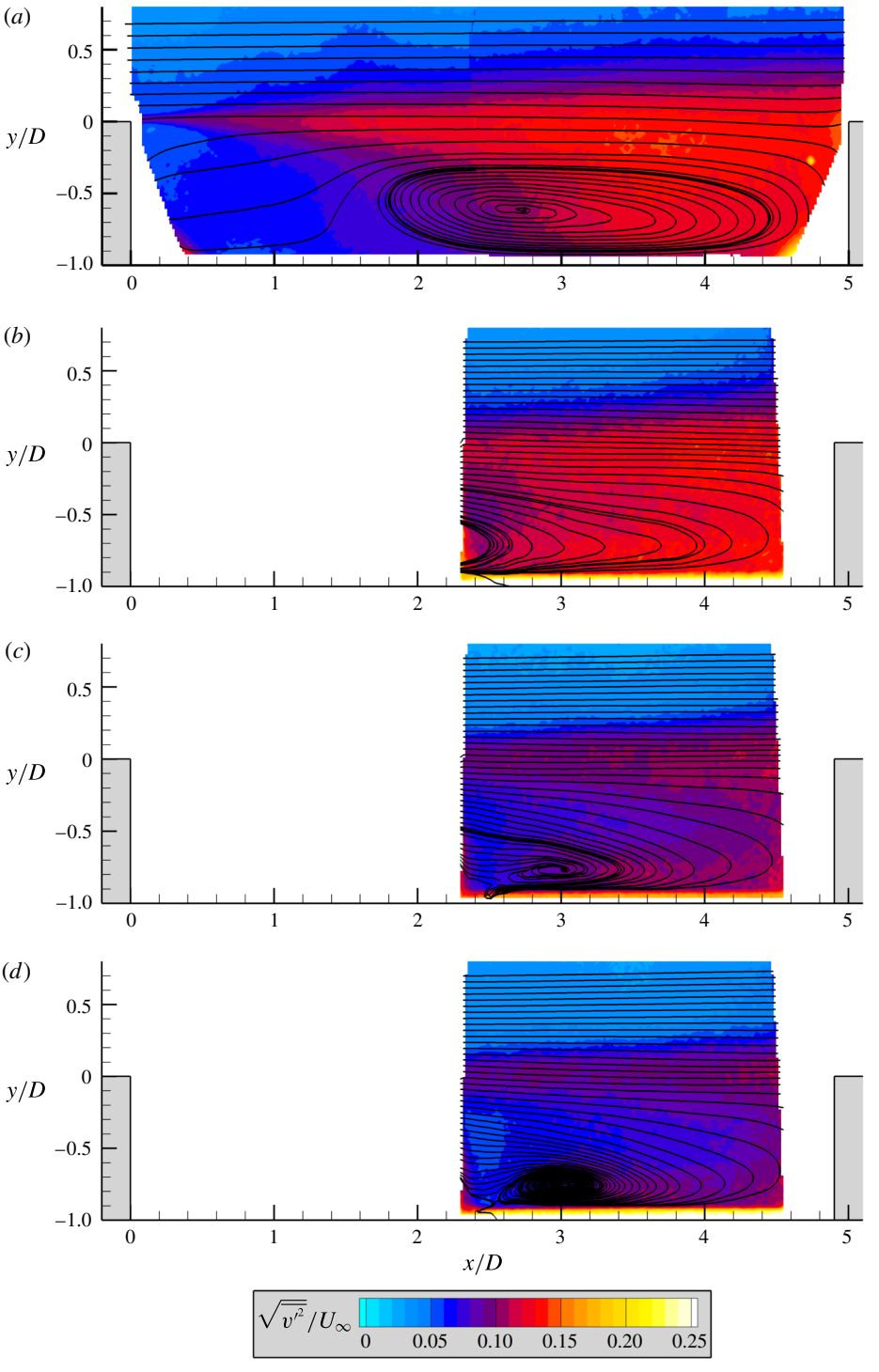


FIGURE 7. (Colour online) As figure 6, but for the 5 × 3 cavity.

https://doi.org/10.1017/jfm.2016.540 Published online by Cambridge University Press

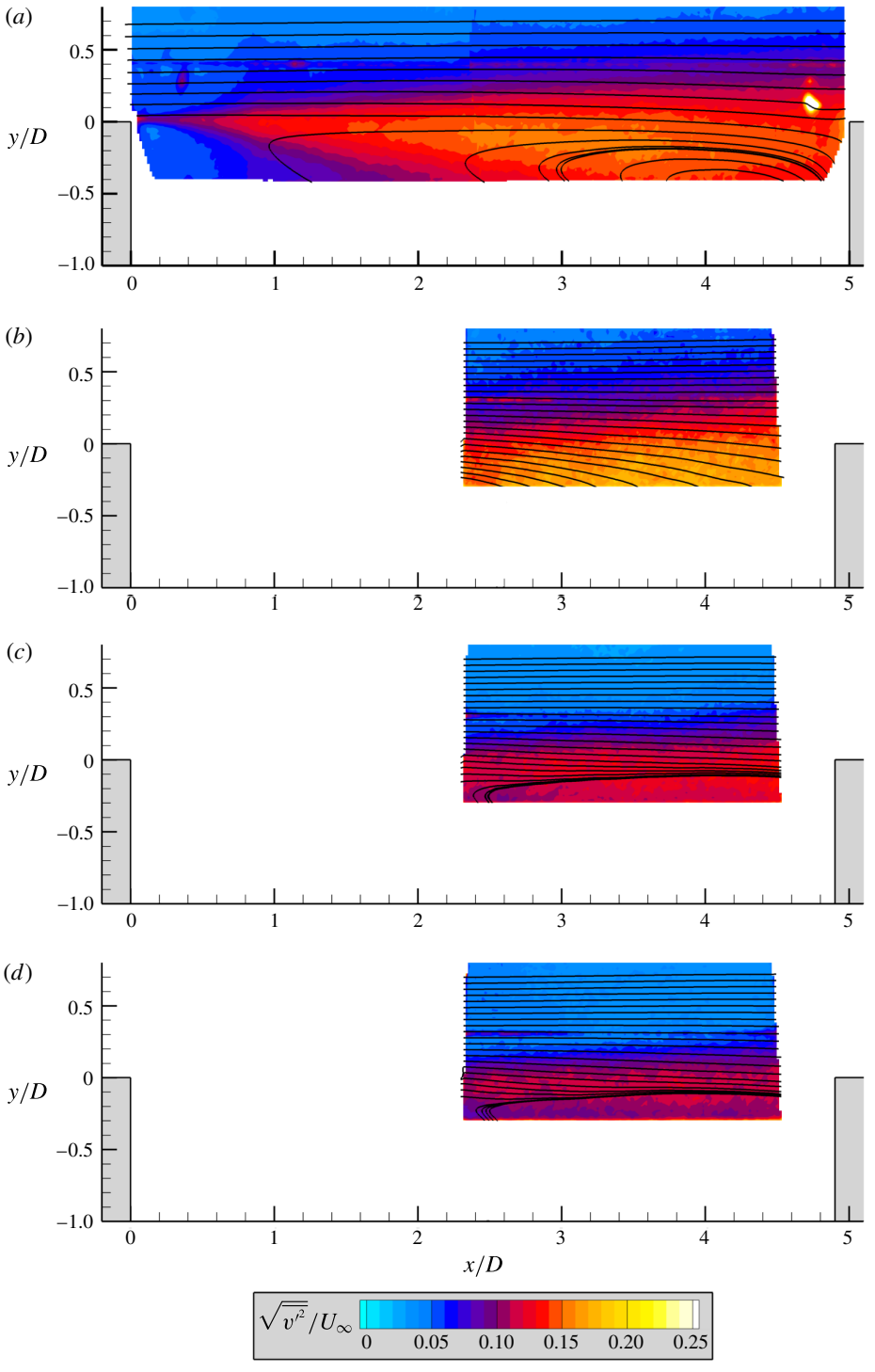


FIGURE 8. (Colour online) As figure 6, but for the 5 × 1 cavity.

https://doi.org/10.1017/jfm.2016.540 Published online by Cambridge University Press

4.4. *Spanwise turbulence intensity*

The spanwise component of the turbulence intensity behaves identically to the vertical component, save that magnitudes are approximately 25 %–30 % greater. The spatial distribution of the turbulence intensity is no different and reduced magnitudes also occur for the 5 × 3 cavity in comparison to the 5 × 5 and 5 × 1 cavities. The compressibility effect is present for the 5 × 3 cavity, in which magnitudes of w' in the shear layer and recirculation region fall as the Mach number reaches 2 and 2.5. Even the small increase in magnitude at Mach 1.5 above the Mach 0.8 levels for the 5 × 1 cavity is observed. Since no new insights are found from w', these figures are omitted for brevity. Some quantities derived from this component will be included in § 5.

4.5. *Turbulent shear stress*

The primary component (streamwise-vertical) of the turbulent shear stress, $u'v'$, is shown in figure 9 for the 5 × 5 cavity. As expected, $u'v'$ is elevated within the shear layer. It is not as prominent in the recirculation region as the normal turbulent stresses were, particularly near the cavity floor. As the Mach number is increased, no significant reduction in turbulent shear stress magnitude is evident, although perhaps a minimal decrease in shear stress may be present for the Mach 2.5 case.

Conversely, compressibility effects on $u'v'$ are distinct for the 5 × 3 cavity in figure 10. The Mach 1.5 magnitudes and extent are perhaps slightly smaller than Mach 0.8, but at Mach 2 and 2.5, $u'v'$ drops markedly in the shear layer and leaves little impression within the recirculation region either. The shear layer is observed to thin as well.

Again, data from the 5 × 1 cavity are omitted. The results for this configuration mimic those of v' shown in figure 8, in which the magnitude of $u'v'$ increases at Mach 1.5 compared to Mach 0.8, then drops slightly at Mach 2 and 2.5 while the extent of the shear layer shrinks to within the limited field of view. Therefore, a compressibility effect can be observed for the 5 × 1 cavity, but not as strongly as for the 5 × 3 cavity.

The maximum non-dimensional turbulent shear stress in the 5 × 5 cavity was measured as 0.015, compared to a value of 0.022 in Murray *et al.*'s (2009) Mach 0.73 experiment in a two-dimensional cavity of similar L/D. Forestier, Jacquin & Geffroy (2003) acquired Mach 0.8 data in a much deeper cavity and reported a maximum turbulent shear stress of approximately 0.02. Incompressible values have ranged from 0.008 to 0.025 (Grace *et al.* 2004; Haigermoser *et al.* 2008; Basley *et al.* 2011).

The remaining two components of the turbulent shear stress are not discussed because their magnitudes are low and the data noisy, which makes it problematic to draw any meaningful conclusions.

5. Turbulence magnitudes

Compressibility effects on turbulent fluctuations can be better examined by using more quantitative comparisons. The conventional means of comparing velocity statistics between the different Mach numbers would be to extract profiles at various streamwise locations and plot them simultaneously. However, that approach is hampered here by small variations in the cavity flow structure as the Mach number changes, as well as the considerably larger variations as a function of cavity width. Although the fundamental structure is consistent across the range of Mach numbers, the position and size of the recirculation region shifts somewhat as does the peak

https://doi.org/10.1017/jfm.2016.540 Published online by Cambridge University Press

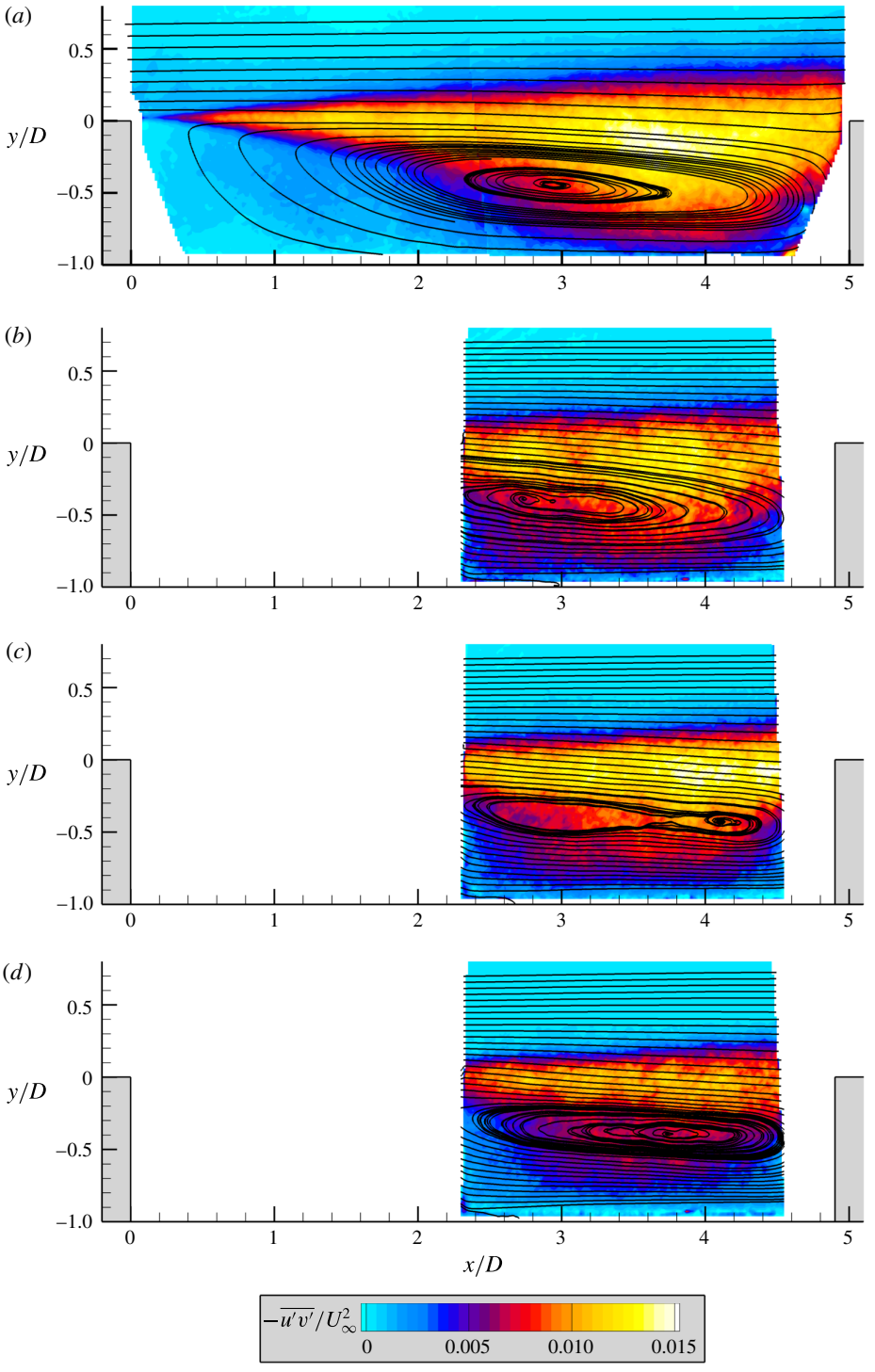


FIGURE 9. (Colour online) Primary turbulent shear stress fields for the 5 × 5 cavity with superposed streamlines derived from the mean velocity field; (*a*) Mach 0.8; (*b*) Mach 1.5; (*c*) Mach 2; (*d*) Mach 2.5.

https://doi.org/10.1017/jfm.2016.540 Published online by Cambridge University Press

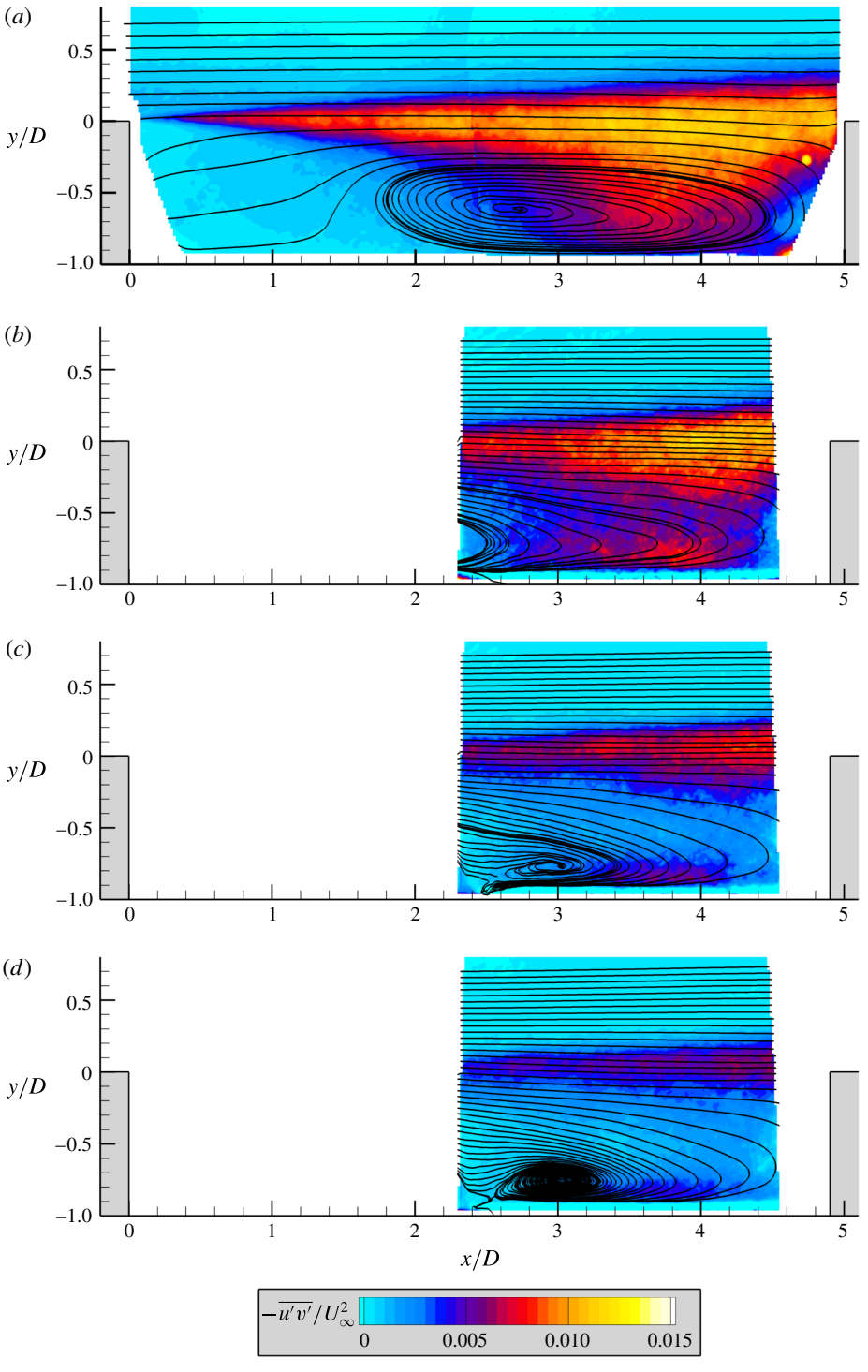


FIGURE 10. (Colour online) As figure 9, but for the 5 × 3 cavity.

https://doi.org/10.1017/jfm.2016.540 Published online by Cambridge University Press

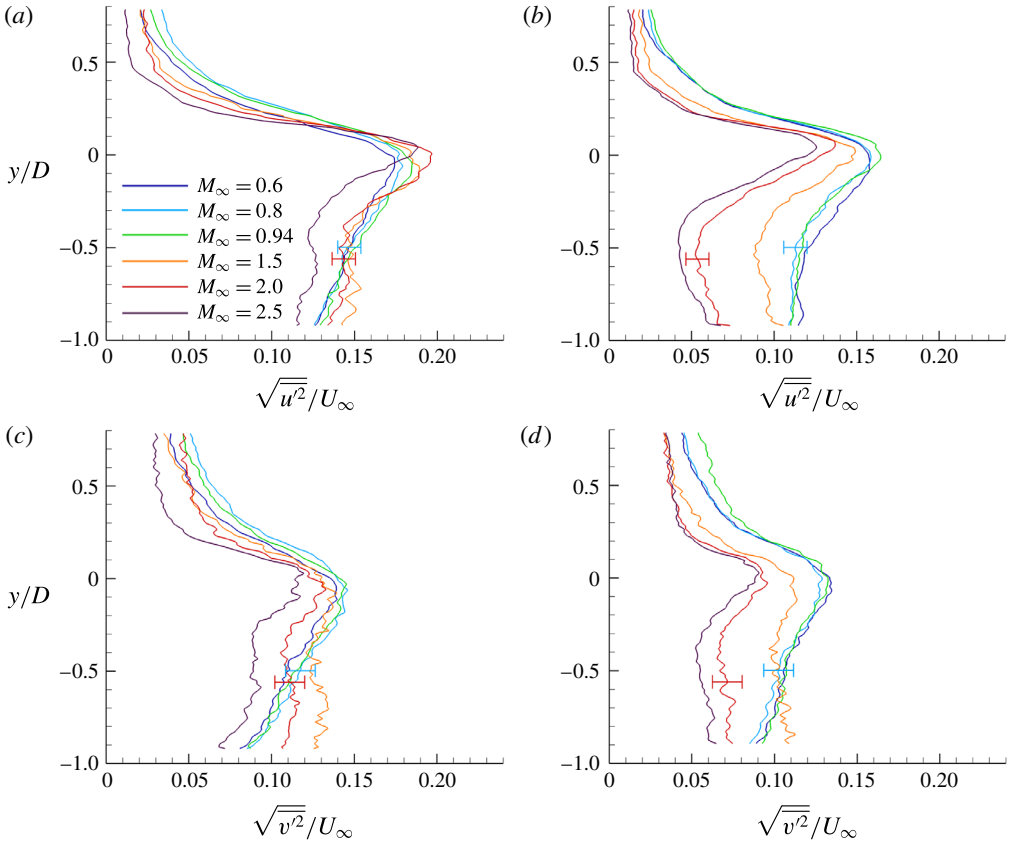


FIGURE 11. (Colour online) Profiles of turbulence intensities at $x/D = 2.45$. (*a*) Streamwise component, 5 × 5 cavity; (*b*) streamwise, 5 × 3; (*c*) vertical component, 5 × 5 cavity; (*d*) vertical, 5 × 3.

position of the shear layer, and this variability interferes with a direct comparison of velocity profiles.

Figure 11 illustrates the challenge. The streamwise component of the turbulence intensity for the 5 × 3 cavity is most straightforward to interpret, shown in figure 11(*b*). Here, it is clear that the three transonic cases exhibit no significant differences but the three supersonic cases show reduced turbulence intensity as the Mach number is raised. The profile shape does not change although the position of the peak tends to drift upwards within the cavity as Mach number is increased. The 5 × 5 cavity in figure 11(*a*) does not offer a clear compressibility effect, although the Mach 2.5 case shows some reduction in turbulence intensity within the recirculation region but not near the shear layer peak. As in the 5 × 3 cavity, the peak position tends to drift upwards as Mach increases but here the peak magnitude does not follow an evident trend. Some difference in profile shape is suggested as well, with the supersonic profiles reaching a more constant value as the cavity floor is approached whereas the transonic cases continue to diminish.

The vertical component of the turbulence intensity displays similar trends but in a manner that exacerbates differences between the transonic and supersonic flow structure. Both the 5 × 5 and 5 × 3 cavities in figure 11(*c*,*d*) show compressibility

https://doi.org/10.1017/jfm.2016.540 Published online by Cambridge University Press

effects in the shear layer. The transonic cases do not indicate a change in peak turbulence intensity but as the Mach number is raised the supersonic cases exhibit a reduction in this quantity; the effect is noticeably stronger for the 5 × 3 cavity. Again, the peak position drifts higher in the shear layer as Mach number rises. As in the streamwise component, the recirculation region manifests differently in the supersonic cases, showing greater constancy as the floor is approached than for the transonic cases. These variations hamper direct comparisons between the different cases.

Although the velocity profiles distinguish compressibility effects in the recirculation region as well as the shear layer, they are restricted to a single streamwise location in the flow unless many profiles are provided. A superior approach to investigate the shear layer in the present data set is to locate the maximum value of each turbulence quantity as a function of streamwise location and plot this for each case. This eases comparison between the various conditions and removes the subjective influence of the recirculation region.

Because second-order statistics such as turbulence quantities become noisy as velocity uncertainties are propagated, each data field was filtered prior to locating the local maxima. A median filter was found to be superior to any smoothing algorithms because the former preserves the edges of the shear layer and prevents artificial thickening or reduction of maxima. The median filter was implemented on a 3 × 3 scalar matrix independently for each component of turbulent stress. Subpixel accuracy was obtained by fitting a second-order polynomial in the vicinity of the peak. The supersonic cases all use the stereoscopic measurements for consistency between configurations.

Figure 12 shows the maxima for four key turbulence quantities measured in the 5 × 5 cavity: the three components of the turbulence intensity and the primary turbulent shear stress. As has been observed previously, compressibility effects are difficult to detect for this cavity width. The only component to show a clear effect is the vertical turbulence intensity, and this is marginal compared to the uncertainty estimate although its consistency with streamwise position suggests it is significant. Therefore, a small reduction in magnitude of v' with rising supersonic Mach number appears valid. The streamwise and spanwise components actually suggest an increase in magnitude for the supersonic cases, but the lack of a uniform trend as a function of Mach number makes this difficult to interpret. Nothing significant may be extracted concerning the turbulent shear stress in figure 12(*d*).

Stronger compressibility effects have been observed in the 5 × 3 cavity and this is again the case in figure 13. All four turbulence quantities indicate a reduction in magnitude for the supersonic cases as the Mach number rises, to an extent that clearly exceeds the measurement uncertainty. The strength of these trends is considerably greater than anything observed for the 5 × 5 cavity. The strongest impact occurs for v' and $u'v'$.

The results for the 5 × 1 cavity, shown in figure 14, are more muddled in comparison to the two wider cavities. This is in part because the mean flow structure of the narrowest cavity differs from the wider configurations (Beresh *et al.* 2015*a*,*b*) and in part because a jump in the turbulence magnitudes occurs in the transition from the transonic cases to the Mach 1.5 case. This is evident in each of the panels of figure 14. However, when the three supersonic cases are considered independently from the transonic data, it is apparent that the magnitudes of each turbulence quantity fall as the Mach number rises, and that these trends exceed the measurement uncertainty. Therefore, there appears to be a significant compressibility

https://doi.org/10.1017/jfm.2016.540 Published online by Cambridge University Press

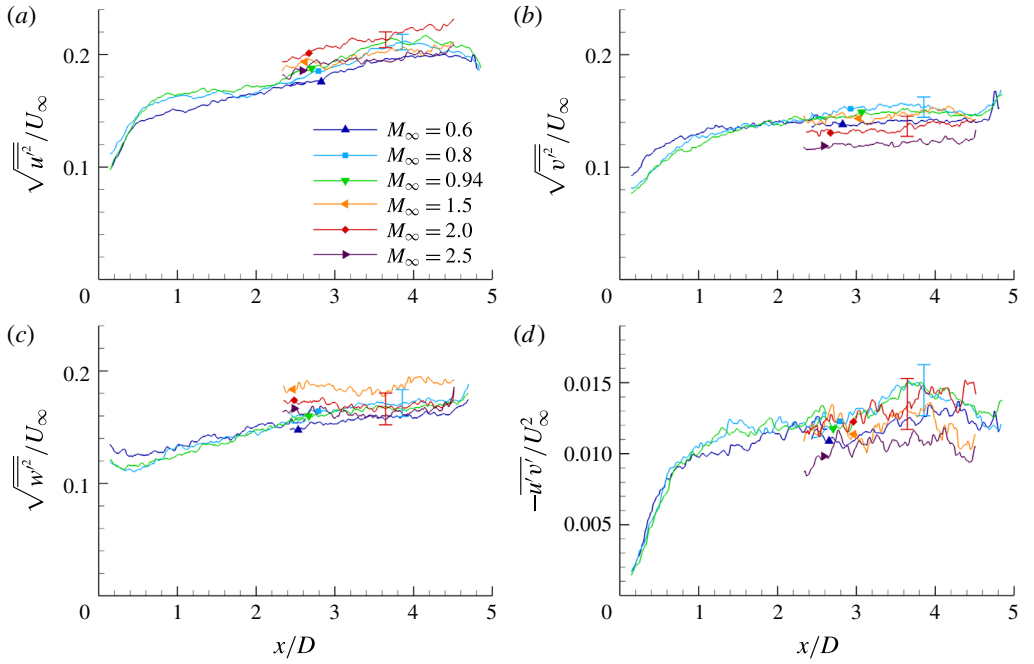


FIGURE 12. (Colour online) Maxima of turbulence quantities as a function of streamwise location for the 5 × 5 cavity at all Mach numbers. (*a*) Streamwise turbulence intensity; (*b*) vertical turbulence intensity; (*c*) spanwise turbulence intensity; (*d*) primary turbulent shear stress.

effect (more so than the 5 × 5 cavity in figure 12) but it is masked by a second effect that raises the turbulence levels in the supersonic cases. The latter may be an experimental artefact related to the smaller confines of the test section used for the supersonic measurements, although it is unclear why this should occur only for the narrowest cavity. Possibly it is related to the lack of spillage vortices in this case. The 5 × 1 cavity also differs in that u' and $u'v'$ appear to peak prior to nearing the aft wall, which is not evident in the 5 × 5 or 5 × 3 cavities, nor does it occur for v' or w'. However, this does not appear to affect the compressibility trends in the three supersonic cases.

Despite the ambiguities, several important points may be gleaned from figures 12–14. Compressibility effects are not observed in the three transonic cases but they become possible once Mach 1.5 is reached. A reduction in magnitude of all three components of the turbulence intensity as well as the primary component of the turbulent shear stress occurs as the Mach number is raised. However, this develops only for the 5 × 3 and 5 × 1 cavities. For the 5 × 5 cavity, a significant compressibility effect is observed only for v' and even this is small. Compressibility effects in the 5 × 3 cavity are stronger than in the 5 × 1 cavity. These trends may all be confirmed by the full field data shown in figures 4–10.

It therefore is clear that the influence of compressibility is a function of the cavity width. Although the cavity width alters the mean structure of the recirculation region, this structure is not meaningfully dependent upon Mach number (Beresh *et al.* 2015*a*) and thus does not appear to contribute to a compressibility effect. Instead, the width dependence of compressibility may be a manifestation of spanwise waveforms

https://doi.org/10.1017/jfm.2016.540 Published online by Cambridge University Press

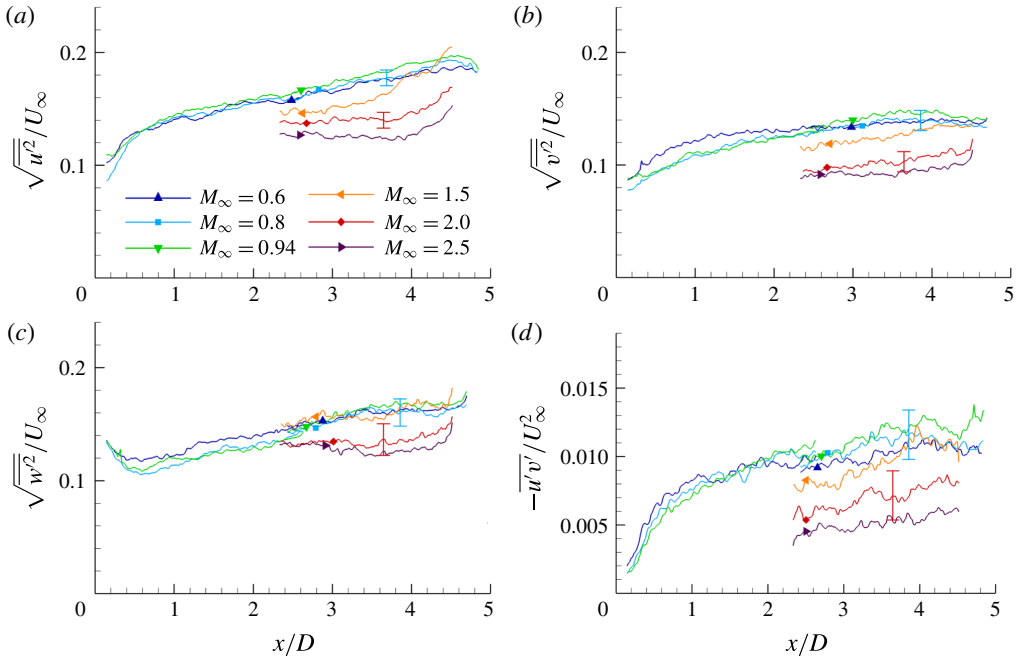


FIGURE 13. (Colour online) As figure 12, but for the 5 × 3 cavity.

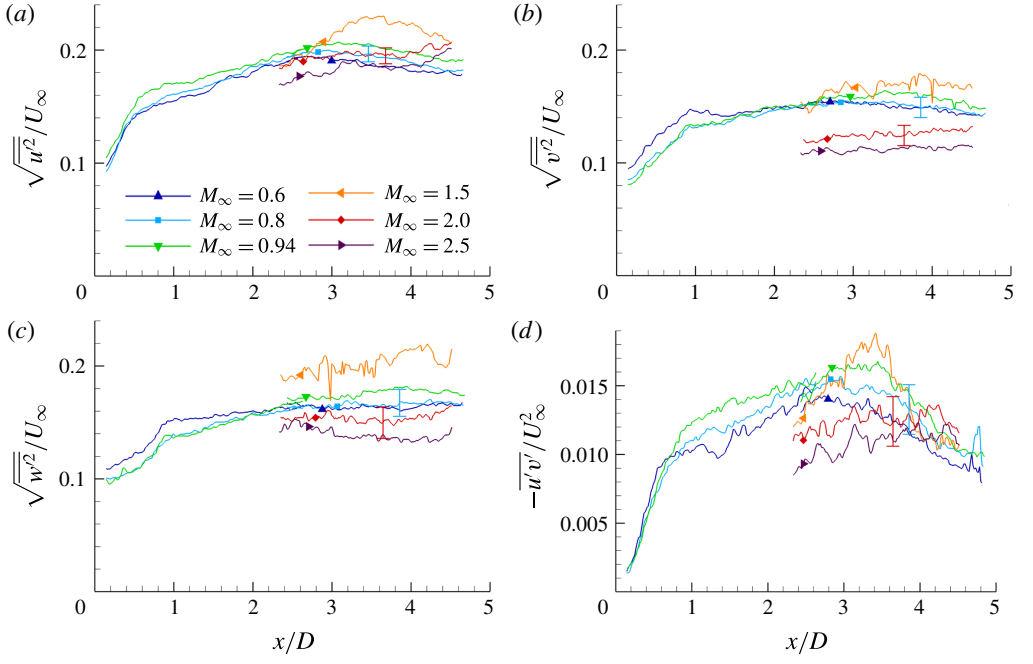


FIGURE 14. (Colour online) As figure 12, but for the 5 × 1 cavity.

dependent on cavity width and known to influence the flow behaviour (e.g. Maull & East 1963; Rockwell & Knisely 1980; Theofilis 2003; Brès & Colonius 2008; Faure

https://doi.org/10.1017/jfm.2016.540 Published online by Cambridge University Press

et al. 2009; Zhang & Naguib 2011). In fact, even free shear layers are known to be subject to a spanwise forcing when side walls are introduced (Morris & Giridharan 1991; Clemens & Mungal 1992) and that the resulting amplification rate is a function of Mach number (Zhuang *et al.* 1990; Robinet, Dussauge & Casalis 2001). This would be consistent with the presently observed behaviour for a shear layer subject to the confines of a cavity and it indicates the presence of an additional instability whose susceptibility to compressibility effects may differ from the usual shear layer instabilities. Moreover, the strength of this instability appears to be dependent upon its wavelength corresponding to the cavity width (Faure *et al.* 2009; Basley *et al.* 2014) or that different oscillatory modes emerge based on the width (de Vicente *et al.* 2014; Douay, Pastur & Lusseyran 2016). Either of these views would offer a mechanism wherein compressibility becomes a function of cavity width. Although the present measurements do not provide direct evidence of this spanwise instability, the effects on the mean flow field structure have been observed previously (Beresh *et al.* 2015*a*,*b*) and a width dependence for the turbulence amplification is consistent. It is not known how the presence of spillage vortices may interact with spanwise instabilities.

An alternative explanation to compressibility effects on turbulence quantities is that the shear layer is forced by the cavity resonance and this forcing diminishes with Mach number as the acoustic tones shift in frequency and amplitude. However, this does not appear to withstand scrutiny of the resonance tones shown in figure 2. For all three cavity widths, the frequencies, and especially amplitudes, of the resonance tones are a function of Mach number for transonic cases. Yet figures 12–14 exhibit no significant variation in the turbulence quantities in the transonic range. In contrast, the resonance amplitudes for the first three modes decrease markedly for supersonic cases in figure 2. This occurs very similarly for all three cavity widths. But again this is inconsistent with the behaviour of the turbulence quantities in figures 12–14, in which cavity width is a dominant factor in how the Mach number influences the flow. These observations suggest that compressibility is a more fitting explanation than acoustic forcing.

The only experiment known to study variation in the turbulence field of a cavity flow as a function of Mach number is that of Murray *et al.* (2009). However, they study Mach numbers reaching only 0.73 and they find that v' and $u'v'$ both rise somewhat as the Mach number increases. This trend is in contrast not only with the present measurements but also with a wealth of knowledge from free shear layer experiments (e.g. Dutton 1997). Furthermore, the free shear layer studies suggest that no noticeable compressibility effect should be observed until the convective Mach number reaches 0.6, which would not have been the case for Murray *et al.*'s experiment. Murray & Elliott (2001) did not acquire quantitative turbulence measurements but their visualizations of turbulent structure suggest that compressibility effects similar to those found in free shear layers may be found in the shear layer over a cavity, albeit with weaker trends. The trends in Murray *et al.* (2009) may actually be with rising Reynolds number rather than rising Mach number, as their experiment did not decouple these parameters.

Lacking sufficient data from cavity flows, comparison with free shear layers may prove informative. Firstly, no compressibility effects are found in the turbulence quantities for the three transonic conditions. Free shear layer studies have suggested that the influence of compressibility should not occur until a convective Mach number M_c of 0.6 has been reached (Sandham & Reynolds 1991; Clemens & Mungal 1995; Elliott *et al.* 1995). In the present case, $M_c = 0.6$ is achieved between Mach 0.94

https://doi.org/10.1017/jfm.2016.540 Published online by Cambridge University Press

and Mach 1.5 (see the analysis in the following section) and therefore it should be expected that compressibility effects will not be observed until supersonic conditions are tested.

The prevailing view from free shear layer studies is that v' and $u'v'$ are considerably diminished as the Mach number increases but u' falls only slightly or not at all (Elliott & Samimy 1990; Goebel & Dutton 1991; Freund *et al.* 2000; Urban & Mungal 2001). The spanwise component w' appears to remain constant (Gruber *et al.* 1993). The present measurements in a cavity shear layer show limited consistency with the free shear layer observations. In the 5×5 cavity, where the weakest compressibility influence is found, v' is the only component to show an effect. This would seem to be consistent with free shear layer data that show this component to be the most strongly affected by compressibility even if the magnitude of the effect is considerably different. The $u'v'$ values do not show a reduction with Mach number as would be suggested by comparison to free shear layers. In contrast, the 5×3 cavity shows a much stronger compressibility effect but a similar degree of impact is found on all three components of turbulent intensity rather than a concentration in v'. The behaviour of the 5×1 cavity is more akin to the 5×3 than the 5×5 cavity. Overall, the trends in the cavity shear layer are not well predicted by those in a free shear layer.

The poor comparison of the turbulent stresses in a cavity shear layer to those in a free shear layer may be because different physical phenomena are at play. The canonical free shear layer is a self-similar flow. The cavity shear layer is not due to the spatially varying lower boundary condition imposed by the recirculation region. Furthermore, free shear layers are subject to boundary conditions that are invariant in the spanwise direction whereas the present cavity flow not only has side-wall effects but also the structure and strength of the recirculation region is a function of the cavity width (Beresh *et al.* 2015*a*,*b*). Therefore similarity should not be expected even between the different cavity geometries. Indeed, figures 12–14 demonstrate that the reduction in turbulence magnitudes with rising Mach number is very different for the three cavity widths that have been tested. As already noted, the interplay between the wavelength of spanwise instabilities and the cavity width is known to affect spanwise flow structure and the amplification of resonances; perhaps its influence may be found in turbulent stresses as well.

6. Shear layer growth rates

6.1. *Cavity flow measurements*

Studies of free shear layers have shown that compressibility leads to a thinning of the vertical extent and a reduction of growth rate (see the discussion in the introduction). Much of the seminal research has determined the thickness of a free shear layer using a threshold rule, in which the thickness of the shear layer is determined between fixed percentage levels of each of the two free stream values. In the case of a cavity shear layer, an ambiguity arises from the presence of the recirculation region on the lower side rather than the uniform stream of a free shear layer. This presents a complication in the selection of an appropriate boundary value, which furthermore will vary along the streamwise axis. A more rigorously defined shear layer scale may be found by using the momentum thickness, which integrates the velocity profile analogously to the boundary layer momentum thickness. This occasionally has been used in cavity flows (Forestier *et al.* 2003; Larchevêque *et al.* 2004) but suffers from an ill-defined lower boundary where the velocity does not trend towards zero owing to the recirculation region.

https://doi.org/10.1017/jfm.2016.540 Published online by Cambridge University Press

A better approach in cavity flows is the vorticity thickness (Rowley *et al.* 2002), $\delta_\omega = (U_1 - U_2)/(\mathrm{d}U/\mathrm{d}y)_{max}$. The use of the velocity gradient presents an unambiguous measure of the thickness without need to consider a boundary threshold. However, a value must be assumed for the lower stream, conventionally achieved simply by setting $U_2 = 0$ (Haigermoser *et al.* 2008; Kang, Lee & Sung 2008; Murray *et al.* 2009; Bian *et al.* 2011; Crook *et al.* 2013). Of course, $U_1 = U_\infty$. The vorticity thickness has the additional advantage for the present experiment that it does not require measurement of the velocity field all the way to the floor of the cavity. The maximum velocity gradient can be expected near the centre of the shear layer and no further penetration into the cavity is necessary. This means that the two-component measurements from the supersonic experiments and the stereoscopic measurements for the 5 × 1 cavity are all sufficient to provide an objective measure of the shear layer thickness.

Figure 15(*a*) shows the vorticity thicknesses for the 5 × 5 cavity at all six Mach numbers as a function of streamwise position in the cavity. Data are available at every x location even for the supersonic cases because the two-component measurements cover the full length of the cavity at this width. Figure 15(*b*) provides the equivalent data for the 5 × 3 cavity but here two-component data exist only for Mach 1.5 amongst the supersonic cases. Therefore, only a limited portion of the cavity has been measured using the stereoscopic data for Mach 2 and 2.5. Finally, figure 15(*c*) shows the vorticity thicknesses for the 5 × 1 cavity, which has no two-component measurements extending the field of view for the supersonic cases.

The vorticity thickness profiles for the 5 × 5 cavity of figure 15(*a*) show several features consistent with previous cavity studies. The shear layer properties may be broken into three regions based on vorticity thickness behaviour (Forestier *et al.* 2003), although some earlier studies have regarded these as only two regions by excluding the rapid decay in thickness near the aft wall (Larchevêque *et al.* 2004; Brès & Colonius 2008; Bian *et al.* 2011). Regardless of this viewpoint, the first region is characterized by fast growth of the shear layer, then the growth slows significantly to mark the onset of the second region, which extends until the aft wall influence is felt. The rapid initial growth of the shear layer is fed by the cavity's acoustic resonances exciting the Kelvin–Helmholtz instability (Gharib & Roshko 1987; Rowley *et al.* 2002). At some point, this instability saturates and the growth of the shear layer tapers off to a lower but approximately constant value, accounting for region 2 (Larchevêque *et al.* 2004). An outlying simulation finds a higher growth rate for the second stage (Brès & Colonius 2008). Some incompressible or weakly compressible cavity flows have measured only a single region of growth, but these appear to occur predominately when conditions create self-sustained oscillations but do not induce resonance (Ashcroft & Zhang 2005; Haigermoser *et al.* 2008; Kang *et al.* 2008; Crook *et al.* 2013). Single-stage growth has been found in resonating compressible flows as well (Rowley *et al.* 2002; Murray *et al.* 2009) and may be a function of a cavity length insufficient to reach saturation of the instability (Rowley *et al.* 2002). Given this diversity of past experiences and flow conditions, the present case is typical of compressible cavity flows, but no unique representative flow field may be identified.

Figure 15(*a*) reveals clear differences in the growth of the 5 × 5 cavity shear layer as a function of Mach number. The three transonic cases all are essentially identical, but compressibility effects become evident for the supersonic cases. In region 1, increasing supersonic Mach number leads to a reduction of the shear layer growth rate. Conversely, region 2 appears to display less dependence on Mach number, but the overall thickness of the shear layer remains reduced at higher Mach numbers

https://doi.org/10.1017/jfm.2016.540 Published online by Cambridge University Press

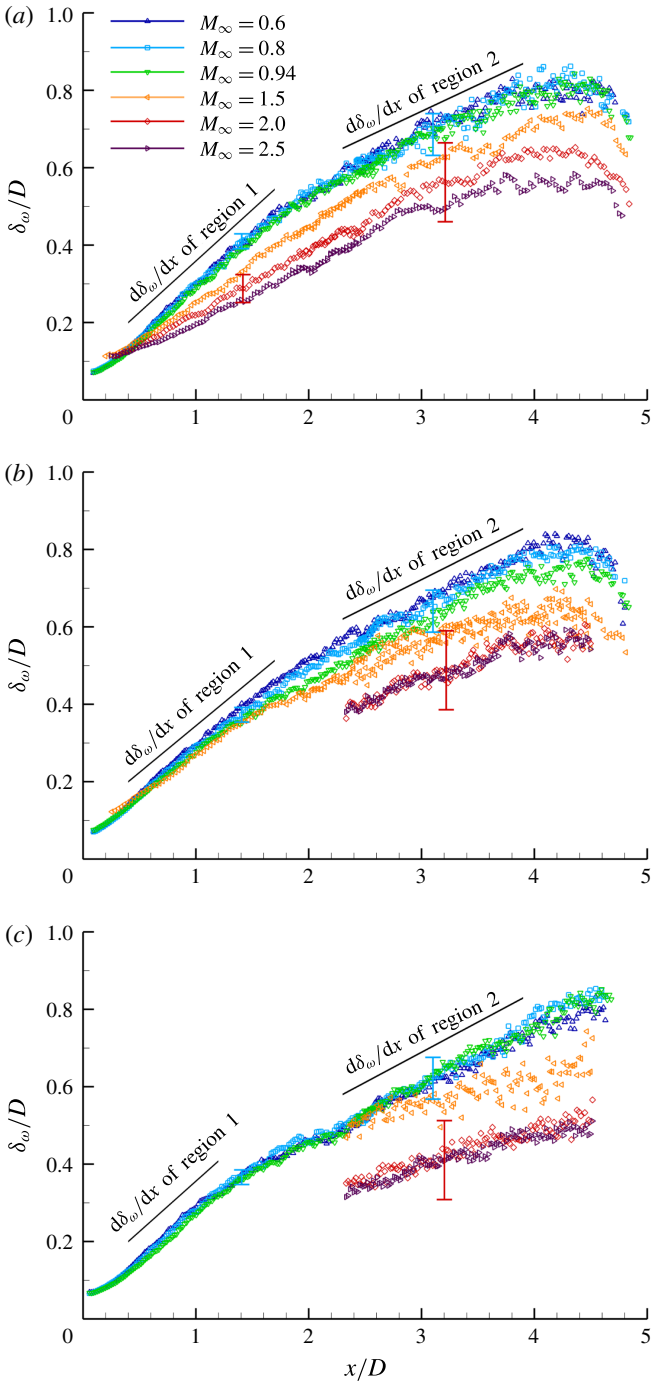


FIGURE 15. (Colour online) Vorticity thickness of the cavity shear layer. Black lines indicate slopes of the region 1 and region 2 growth rates. (*a*) 5 × 5 cavity; (*b*) 5 × 3 cavity; (*c*) 5 × 1 cavity.

https://doi.org/10.1017/jfm.2016.540 Published online by Cambridge University Press

due to the continuing impact of region 1. The behaviour in region 1 is precisely that which has been well established from numerous compressible free shear layer experiments. No effect comparable to region 2 is found from free shear layer studies since the latter do not exhibit saturation of the shear layer instability as may occur in cavity flows.

Figure 15 includes sample uncertainty estimates for the vorticity thickness at two representative Mach numbers and in each region. The uncertainties of the vorticity thicknesses were propagated from the velocity uncertainties using a Taylor expansion. This results in a large uncertainty downstream where the gradient in the mean velocity profile is smaller, which appears overly conservative in region 2 given that it greatly exceeds the random variations in δ_ω that are observed. The uncertainty is larger still for the supersonic cases because of the fewer number of vector fields and therefore greater convergence uncertainty. However, the data appear better behaved than is suggested by the uncertainty estimates, which do not account for trends through numerous data points. The variation of δ_ω as a function of Mach number is quite distinct despite lying within the uncertainty band and is highly likely to be significant.

Data for the 5 × 3 cavity are supplied in figure 15(*b*) and they exhibit some differences in comparison to the 5 × 5 cavity. Region 1 measurements are not available for the two higher Mach numbers, but the transonic data alone suggest a different trend. Whereas the 5 × 5 cavity did not show any change in the region 1 growth rate for the three transonic cases, the 5 × 3 cavity suggests a diminishing growth rate as the transonic Mach number is increased. The single available supersonic case continues this trend. In region 2, growth rates are all approximately equal, as was also the case for the 5 × 5 cavity. The lower overall vorticity thicknesses for Mach 2 and Mach 2.5 in region 2, despite common slopes, suggests that the growth rate in region 1 must have been lower still for these cases.

The behaviour of the 5 × 1 cavity is again different. Here, the region 1 growth rates are identical for the three transonic cases, but the region 2 growth rates appear to show lower values for the supersonic cases as compared to transonic. Moreover, region 1 terminates earlier than for the 5 × 5 and 5 × 3 cavities, suggesting that the instability saturates more rapidly. The 5 × 1 data do not extend quite as far downstream as for the two wider cavities because the limited field of view interferes with evaluation of the vorticity thickness near the aft wall.

The growth rates may be found by determining the slopes of the vorticity thickness plots in each of the first two regions, with the results presented in figure 16. Region 1 is defined as $0.4 < x/D < 1.7$ for the 5 × 5 and 5 × 3 cavities but shortened to $0.4 < x/D < 1.2$ for the 5 × 1 cavity, based on linearity of the plots in figure 15. Region 2 is $2.3 < x/D < 3.9$ in all cases. A simple least-squares fit was used to calculate the shear layer growth rate $\mathrm{d}\delta_\omega/\mathrm{d}x$. Uncertainties were estimated based upon the quality of the fit, which in turn is a function of the degree of scatter of the data points.

The most complete data for region 1 are those of the 5 × 5 cavity. The three transonic cases show minimal variation in growth rate, but once supersonic conditions are reached a considerable reduction in growth rate occurs as the Mach number rises. The 5 × 3 cavity differs in that the transonic growth rates are lower than those of the 5 × 5 cavity and show a diminishing trend with increased Mach number even at these weakly compressible conditions. The single data point for a supersonic case in the 5 × 3 cavity closely matches its 5 × 5 counterpart. The three available transonic data points for the 5 × 1 cavity agree well with the 5 × 5 data.

The region 2 growth rates drop significantly for Mach 1.5 as compared to the transonic cases, but then rise slightly for Mach 2 and 2.5. This is true for all

https://doi.org/10.1017/jfm.2016.540 Published online by Cambridge University Press

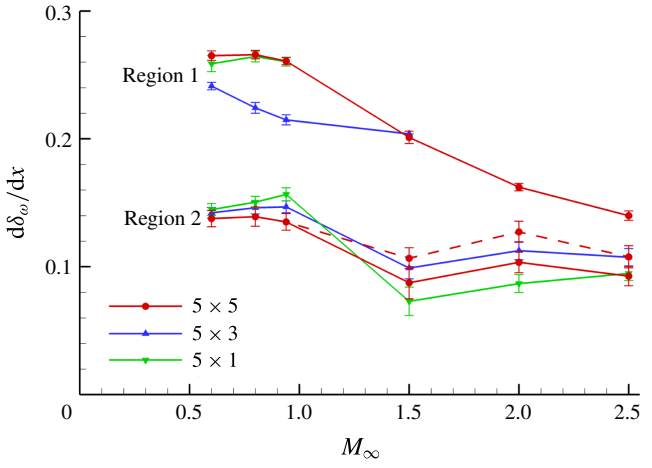


FIGURE 16. (Colour online) Growth rates of the cavity shear layer for each of the cavity widths. Supersonic data in region 2 are shown in solid lines for stereoscopic measurements and a dashed line for two-component measurements.

three cavity widths. Overall, no clear or strong trend is evident for region 2 and it is reasonable to conclude that the growth rate is approximately constant for all conditions following saturation of the instability. Yet the shear layer thickness clearly decreases with increasing supersonic Mach number for all three cavity widths, as evidenced in figure 15. This implies that the region 1 growth rate must diminish appreciably as Mach number increases for all three cavity widths, which makes the absence of supersonic measurements in this region unfortunate for the narrower two cavities. Nevertheless, this observation helps confirm that region 1 growth rates fall with rising supersonic Mach numbers even where direct measurements are absent.

Finally, for the 5 × 5 cavity, region 2 data can be determined from both two-component and stereoscopic measurements. A small absolute difference is observed between the two in figure 16, but trends are consistent and no reconsideration of any conclusions would be warranted.

The region 1 growth rates should be most comparable to the growth rates of free shear layers. The classic compressibility effect found in free shear layers is that increasing Mach number reduces the growth rate, and that trend clearly is replicated for the cavity shear layer in region 1. A comparison of the magnitude of the growth rates is more challenging given the considerable scatter of the data found in the literature. This is the case even for incompressible shear layers. Smits & Dussauge (2006) ultimately concluded that a constant-density free shear layer with $U_2 = 0$ most probably has a growth rate of $d\delta_\omega/dx = 0.16$, although they note the considerable scatter of approximately 35 % found in the data due to sensitivity of the instability to experimental conditions.

In the present case, the incompressible growth rate is $d\delta_\omega/dx = 0.26$, based on the relatively constant trend for the three transonic cases in the 5 × 5 and 5 × 1 cavities. The trend of the 5 × 3 cavity can plausibly be found consistent with this value. This growth rate exceeds the free shear layer value of 0.16 by nearly twice its 35 % scatter. Other cavity studies demonstrate even larger scatter. Some incompressible studies are fairly close to the 0.16 value for free shear layers (Ashcroft & Zhang 2005; Haigermoser *et al.* 2008; Murray *et al.* 2009). Conversely, Rowley *et al.* (2002) and

https://doi.org/10.1017/jfm.2016.540 Published online by Cambridge University Press

Brès & Colonius (2008) find values as low as 0.03 and Kang *et al.* (2008) find the largest known growth rate of 0.37. Certainly, differing experimental conditions play a role, as the growth rate is a function of the cavity length (Sarohia 1977; Rowley *et al.* 2002; Brès & Colonius 2008); with a contrasting opinion by Ashcroft & Zhang (2005) and the state of the incoming boundary layer (Rowley *et al.* 2002; Brès & Colonius 2008; Haigermoser *et al.* 2008). Additionally, Crook *et al.* (2013) notes growth rate can vary when measurements are made off the centreline in a rectangular cavity.

Differences in growth rates amongst the variety of experiments and computations also may be attributable to differences in the resonance amplitudes or their match with the frequency of the Kelvin–Helmholtz instability. This would lead to variations in the energy forcing the instability growth. Alternatively, the receptivity of the instability may vary amongst the flow fields, as this property is known to be sensitive to boundary conditions (Ragab & Wu 1989; Morris & Giridharan 1991; Day, Reynolds & Mansour 1998; Barone & Lele 2005) and therefore would vary amongst the differing experimental conditions of the cavity studies considered.

6.2. *Comparison to free shear layers*

Part of the reason for any ambiguities in the cavity shear layer growth may be that, thus far, they have been studied in terms of the free stream Mach number rather than the convective Mach number, M_c. Studies of free shear layers have well established that use of the convective Mach number of the flow better establishes similarity (Lele 1994; Dutton 1997; Smits & Dussauge 2006), as originally proposed by Bogdanoff (1983) and Papamoschou & Roshko (1988). The convective Mach number is more difficult to determine in the present case because the slow side of the shear layer is bounded by the recirculation region in the cavity as opposed to a uniform free stream, but the assumption of $U_2 = 0$ that was used to calculate the vorticity thickness may be redeployed here. A similar difficulty is encountered in the shear layer over a base flow and the convective Mach number still can be reasonably estimated to find similarity in the data (Dutton 1997).

To properly assess the effect of compressibility on the shear layer growth rate, it must be normalized to its incompressible value. This poses something of a challenge in the present case given that the experiments were conducted exclusively in the compressible regime and no other known incompressible cavity experiments exactly replicate the current finite-width geometries. This is an important consideration, as the current data have shown that the changes to the cavity width affect the shear layer properties. Moreover, as Murray *et al.* (2009) point out, incompressible cavities of the current dimensional range often do not resonate, and this appears to alter the shear layer growth rate.

Figure 16 suggests that a reasonable choice of the incompressible cavity growth rate in region 1 can be extrapolated as 0.26, as noted in § 6.1. This value is used to normalize the measured compressible shear layer growth rates reported in figure 16. The growth rate of free shear layers as a function of the convective Mach number has been assembled previously by several authors (e.g. Lele 1994; Dutton 1997; Smits & Dussauge 2006). In each case, the normalized growth rate $\Phi = (\mathrm{d}\delta_\omega/\mathrm{d}x)/(\mathrm{d}\delta_\omega/\mathrm{d}x)_{incompressible}$ and is plotted as a function of M_c.

Figure 17 reproduces the free shear layer compilation of Smits & Dussauge (2006), which is probably the most complete survey of the available data. Growth rates may differ somewhat from the values reported by the original authors as Smits and Dussauge incorporate subsequent reassessments of the data. The trend of decreasing

https://doi.org/10.1017/jfm.2016.540 Published online by Cambridge University Press

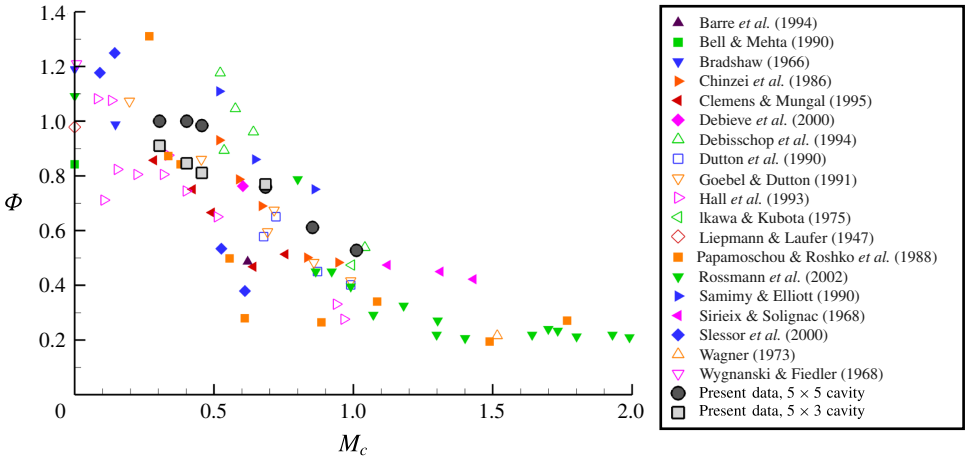


FIGURE 17. (Colour online) Normalized growth rates of region 1 of the cavity shear layer as a function of convective Mach number, superposed on values from free shear layers. After Smits & Dussauge (2006).

normalized growth rate with convective Mach number is strongly evident, even within the substantial scatter of the data. Some of this scatter is attributable to the disparate experimental means of measuring the shear layer thickness (Smits & Dussauge 2006; Barone, Oberkampf & Blottner 2006).

The present cavity data are superposed on the free shear layer data in figure 17. Region 1 growth rates are comparable to those from free shear layers because the physical processes are expected to be similar before the instability saturates in region 2, which is not known to occur in free shear layers. The most complete data are those for the 5 × 5 cavity and these are observed to faithfully follow the free shear layer trends. The 5 × 3 cavity data also are well within the bounds of the free shear layer data. The 5 × 1 case is excluded because region 1 measurements are not available for Mach numbers at which compressibility effects are observed. Smits & Dussauge (2006) noted that shear layer thicknesses determined using the velocity field tend to produce values of Φ towards the higher end of the scatter, and in fact the present measurements lie somewhat greater than the general centroid of the data points. Therefore, the classic compressibility effect on free shear layer growth has been confirmed in the present cavity shear layer data as well. It is interesting to note that the cavity shear layer growth rates well match those from free shear layers despite the absence of good agreement in the turbulence quantities analysed in the previous section.

Free shear layer studies have suggested that the compressible reduction of shear layer growth occurs predominantly above $M_c = 0.6$, at which point the instability mechanism may shift away from the classic Kelvin–Helmholtz instability (Sandham & Reynolds 1991; Clemens & Mungal 1995; Elliott *et al.* 1995). This appears to be the case for the present cavity data as well, but only for the 5 × 5 cavity. The 5 × 3 cavity is not consistent with this trend and displays a falling growth rate across all measured Mach numbers, which may suggest a different instability is operative for this cavity width. The inference of a stronger spanwise instability in the 5 × 3 cavity would be supported by the earlier observations regarding turbulent stresses in § 5. Interestingly, figure 15(*a*,*b*) shows that the shift from region 1 growth to

https://doi.org/10.1017/jfm.2016.540 Published online by Cambridge University Press

region 2 growth is consistent across all Mach numbers, which may suggest that the mechanisms for cavity shear layer growth do not exhibit a change around $M_c = 0.6$, regardless of the clear suppression of the growth rate.

7. Conclusions

The flow over a finite-width rectangular cavity has been studied across a range of free stream Mach numbers from 0.6 to 2.5 to determine the influence of compressibility. This corresponds to an estimated convective Mach number of the cavity shear layer reaching 1.01. The length-to-depth ratio of the cavity was fixed at 5 and three cavity widths were tested to investigate the influence of the length-to-width ratio. The present analysis primarily uses particle image velocimetry data collected as part of previously reported experimental campaigns (Beresh *et al.* 2015*a*,*b*), in which measurements were acquired in the streamwise/wall-normal plane along the centreline of the cavity. Supplemental high-frequency pressure measurements were used to characterize the acoustic environment of the cavity, showing multiple resonance tones whose non-dimensional frequencies diminish with increasing Mach number.

Mean velocity fields reveal that the structure of the recirculation region is essentially invariant with Mach number but differs for the three cavity widths. Measurements of the turbulent stresses also show different behaviour based on cavity width. The widest cavity exhibits a significant compressibility effect only in the vertical component of the turbulence intensity, in which values of this term diminish modestly as Mach number rises. The two narrower cavities show a more substantial drop in all three components of the turbulence intensity as well as the turbulent shear stress. These observations stand in contrast to velocimetry measurements made in canonical free shear layers, which show that the vertical component and the turbulent shear stress are reduced as the Mach number increases but the streamwise and spanwise components are minimally affected (Elliott & Samimy 1990; Goebel & Dutton 1991; Gruber *et al.* 1993; Freund *et al.* 2000; Urban & Mungal 2001). The relative importance of a spanwise instability may explain the dependence of compressibility effects upon the cavity width. One similarity between free shear layers and cavity shear layers is that these compressibility effects on turbulence quantities are initiated only once the convective Mach number exceeds approximately 0.6.

The growth of the cavity shear layer was determined using mean streamwise velocity fields. The vorticity thickness grows rapidly as the shear layer initially develops, then transitions to a slower growth rate once its instability saturates; finally, it falls quickly when the aft wall is neared. Growth rates are approximately constant with streamwise distance in each region and were calculated from the slope of the vorticity thickness. The initial growth rate in the widest cavity falls sharply as a function of Mach number once a convective Mach number of 0.6 is surpassed, but an onset of the growth rate reduction below this Mach number is possible for a narrower cavity. Post-saturation growth rates are approximately constant with Mach number for all three cavity widths. The growth rates prior to saturation were normalized by their estimated incompressible values and plotted against convective Mach number. Showing excellent agreement with the comparable free shear layer data compiled by Smits & Dussauge (2006), the cavity shear layer displays the classic compressibility effect of suppression of its growth rate as the convective Mach number rises. The specific trend of the reduction in growth rate due to compressibility is modified by the cavity width.

The primary question remaining from the present study concerns the source of the cavity width effect upon the compressibility. Only a speculative answer has

https://doi.org/10.1017/jfm.2016.540 Published online by Cambridge University Press

been possible using the available data. Spanwise instabilities are not known to have been experimentally detected in compressible cavity flows, but details concerning their amplification as a function of their wavelength and the Mach number have the potential to explain the current data. It also is not entirely clear how the acoustic resonances in the cavity may force shear layer instabilities and overlap compressibility effects on the turbulence properties. Circumstantial evidence suggests that compressibility better explains the observed suppression of turbulent fluctuations than does forcing, but the latter effect may be present as well. Future experiments can be crafted to isolate these parameters independently from the Mach number.

Acknowledgements

The authors would like to thank S. Arunajatesan, M. Barone, and E. DeMauro, all of Sandia, for numerous discussions of cavity flow physics and their helpful comments on the data and their interpretation. This work is supported by Sandia National Laboratories and the United States Department of Energy. Sandia is a multiprogram laboratory managed and operated by Sandia Corporation, a wholly owned subsidiary of Lockheed Martin Corporation, for the United States Department of Energy's National Nuclear Security Administration under contract DE-AC04-94AL85000.

REFERENCES

AHUJA, K. K. & MENDOZA, J. 1995 Effects of cavity dimensions, boundary layer, and temperature on cavity noise with emphasis on benchmark data to validate computational aeroacoustic codes. *NASA Contractor Rep.* 4653.

ARUNAJATESAN, S., BARONE, M. B., WAGNER, J. L., CASPER, K. M. & BERESH, S. J. 2014 Joint experimental/computational investigation into the effects of finite width on transonic cavity flow. *AIAA Paper* 2014-3027.

ASHCROFT, G. & ZHANG, X. 2005 Vortical structures over rectangular cavities at low speed. *Phys. Fluids* **17** (1), 015104.

BARONE, M. F. & LELE, S. K. 2005 Receptivity of the compressible mixing layer. *J. Fluid Mech.* **540**, 301–335.

BARONE, M. F., OBERKAMPF, W. L. & BLOTTNER, F. G. 2006 Validation case study: prediction of compressible turbulent mixing layer growth rate. *AIAA J.* **44** (7), 1488–1497.

BARRE, S., QUINE, C. & DUSSAUGE, J. P. 1994 Compressibility effects on the structure of supersonic mixing layers: experimental results. *J. Fluid Mech.* **259**, 47–78.

BASLEY, J., PASTUR, L. R., DELPRAT, N. & LUSSEYRAN, F. 2013 Space-time aspects of a three-dimensional multi-modulated open cavity flow. *Phys. Fluids* **25** (6), 064105.

BASLEY, J., PASTUR, L. R., LUSSEYRAN, F., FAURE, T. M. & DELPRAT, N. 2011 Experimental investigation of global structures in an incompressible cavity flow using time-resolved PIV. *Exp. Fluids* **50** (4), 905–918.

BASLEY, J., PASTUR, L. R., LUSSEYRAN, F., SORIA, J. & DELPRAT, N. 2014 On the modulating effect of three-dimensional instabilities in open cavity flows. *J. Fluid Mech.* **759**, 546–578.

BELL, J. H. & MEHTA, R. D. 1990 Development of a two-stream mixing layer from tripped and untripped boundary layers. *AIAA J.* **28** (12), 2034–2042.

BERESH, S. J., WAGNER, J. L., PRUETT, B. O. M., HENFLING, J. F. & SPILLERS, R. W. 2015*a* Supersonic flow over a finite-width rectangular cavity. *AIAA J.* **53** (2), 296–310.

BERESH, S. J., WAGNER, J. L., PRUETT, B. O. M., HENFLING, J. F. & SPILLERS, R. W. 2015*b* Width effects in transonic flow over a rectangular cavity. *AIAA J.* **53** (12), 3831–3834.

BIAN, S., DRISCOLL, J. F., ELBING, B. R. & CECCIO, S. L. 2011 Time resolved flow-field measurements of a turbulent mixing layer over a rectangular cavity. *Exp. Fluids* **51** (1), 51–63.

https://doi.org/10.1017/jfm.2016.540 Published online by Cambridge University Press

BOGDANOFF, D. W. 1983 Compressibility effects in turbulent shear layers. *AIAA J.* **21** (6), 926–927.

BRADSHAW, P. 1966 The effect of initial conditions on the development of a free shear layer. *J. Fluid Mech.* **26** (2), 225–236.

BRÈS, G. A. & COLONIUS, T. 2008 Three-dimensional instabilities in compressible flow over open cavities. *J. Fluid Mech.* **599**, 309–339.

CHINZEI, N., MASUYA, G., KOMURO, T., MURAKAMI, A. & KUDOU, K. 1986 Spreading of two-stream supersonic turbulent mixing layers. *Phys. Fluids* **29** (5), 1345–1347.

CHUNG, K.-M. 2001 Three-dimensional effect on transonic rectangular cavity flows. *Exp. Fluids* **30** (5), 531–536.

CLARK, R. L., KAUFMAN, L. G. II & MACIULAITUS, A. 1980 Aeroacoustic measurements for Mach .6 to 3.0 flows past rectangular cavities. *AIAA Paper* 80-0036.

CLEMENS, N. T. & MUNGAL, M. G. 1992 Effects of sidewall disturbances on the supersonic mixing layer. *AIAA J.* **8** (1), 249–251.

CLEMENS, N. T. & MUNGAL, M. G. 1995 Large-scale structure and entrainment in the supersonic mixing layer. *J. Fluid Mech.* **284**, 171–216.

CROOK, S. D., LAU, T. C. W. & KELSO, R. M. 2013 Three-dimensional flow within shallow, narrow cavities. *J. Fluid Mech.* **735**, 587–612.

DAY, M. J., REYNOLDS, W. C. & MANSOUR, N. N. 1998 The structure of the compressible reacting mixing layer: insights from linear stability analysis. *Phys. Fluids* **10** (4), 993–1007.

DEBIÈVE, J.-F., DUPONT, P., LAURENT, H., MENAA, M. & DUSSAUGE, J.-P. 2000 Compressibility and structure of turbulence in supersonic shear layers. *Eur. J. Mech. (*B*/Fluids)* **19** (5), 597–614.

DEBISSCHOP, J. R., CHAMBRES, O. & BONNET, J. P. 1994 Velocity field characteristics in supersonic mixing layers. *Exp. Therm. Fluid Sci.* **9** (2), 147–155.

DISIMILE, P. J., TOY, N. & SAVORY, E. 2000 Effect of planform aspect ratio on flow oscillations in rectangular cavities. *Trans. ASME* **122** (1), 32–38.

DOUAY, C. L., PASTUR, L. R. & LUSSEYRAN, F. 2016 Centrifugal instabilities in an experimental open cavity flow. *J. Fluid Mech.* **788**, 670–694.

DUDLEY, J. G. & UKEILEY, L. 2011 Detached eddy simulation of a supersonic cavity flow with and without passive flow control. *AIAA Paper* 2011-3844.

DUTTON, J. C. 1997 Compressible turbulent free shear layers. *AGARD Rep.* 819. Turbulence in Compressible Flows, 2-1 to 2-42.

DUTTON, J. C., BURR, R. F., GOEBEL, S. G. & MESSERSMITH, N. L. 1990 Compressibility and mixing in turbulent free shear layers. In *Proceedings of the Twelfth Biennial Symposium on Turbulence*, pp. A22-1 to A22-12.

ELLIOTT, G. S. & SAMIMY, M. 1990 Compressibility effects in free shear layers. *Phys. Fluids* A **2** (7), 1231–1240.

ELLIOTT, G. S., SAMIMY, M. & ARNETTE, S. A. 1995 The characteristics and evolution of large-scale structures in compressible mixing layers. *Phys. Fluids* **7** (4), 864–876.

FAURE, T. M., PASTUR, L., LUSSEYRAN, F., FRAIGNEAU, Y. & BISCH, D. 2009 Three-dimensional centrifugal instabilities development inside a parallelepipedic open cavity of various shape. *Exp. Fluids* **47** (3), 395–410.

FORESTIER, N., JACQUIN, L. & GEFFROY, P. 2003 The mixing layer over a deep cavity at high-subsonic speed. *J. Fluid Mech.* **465**, 101–145.

FREUND, J. B., LELE, S. K. & MOIN, P. 2000 Compressibility effects in a turbulent annular mixing layer. Part 1. Turbulence and growth rate. *J. Fluid Mech.* **421**, 229–267.

GAI, S. L., KLEINE, H. & NEELY, A. J. 2015 Supersonic flow over a shallow open rectangular cavity. *J. Aircraft* **52** (2), 609–616.

GHARIB, M. & ROSHKO, A. 1987 The effect of flow oscillations on cavity drag. *J. Fluid Mech.* **177**, 501–530.

GOEBEL, S. G. & DUTTON, J. C. 1991 Experimental study of compressible turbulent mixing layers. *AIAA J.* **29** (4), 538–546.

GRACE, S. M., DEWAR, W. G. & WROBLEWSKI, D. E. 2004 Experimental investigation of the flow characteristics within a shallow wall cavity for both laminar and turbulent upstream boundary layers. *Exp. Fluids* **36** (5), 791–804.

https://doi.org/10.1017/jfm.2016.540 Published online by Cambridge University Press

GRUBER, M. R., MESSERSMITH, N. L. & DUTTON, J. C. 1993 Three-dimensional velocity field in a compressible mixing layer. *AIAA J.* **31** (11), 2061–2067.

HAIGERMOSER, C., VESELY, L., NOVARA, M. & ONORATO, M. 2008 A time-resolved particle image velocimetry investigation of a cavity flow with a thick incoming turbulent boundary layer. *Phys. Fluids* **20** (10), 105101.

HALL, J. L., DIMOTAKIS, P. E. & ROSEMANN, H. 1993 Experiments in nonreacting compressible shear layers. *AIAA J.* **31** (12), 2247–2254.

HELLER, H. H. & BLISS, D. B. 1975 The physical mechanism for flow-induced pressure fluctuations in cavities and concepts for their suppression. *AIAA Paper* 75-491.

IKAWA, H. & KUBOTA, T. 1975 Investigation of supersonic turbulent mixing layer with zero pressure gradient. *AIAA J.* **13** (5), 566–572.

KANG, W., LEE, S. B. & SUNG, H. J. 2008 Self-sustained oscillations of turbulent flows over an open cavity. *Exp. Fluids* **45** (4), 693–702.

KRISHNAMURTY, K. 1955 Acoustic radiation from two-dimensional rectangular cut-outs in aerodynamic surfaces. *NACA TN* 3487.

LARCHEVÊQUE, L., SAGAUT, P., THIEN-HIEP, L. & COMTE, P. 2004 Large-eddy simulation of a compressible flow in a three-dimensional open cavity at high Reynolds number. *J. Fluid Mech.* **516**, 265–301.

LARCHEVÊQUE, L., SAGAUT, P. & LABBÉ, O. 2007 Large-eddy simulation of a subsonic cavity flow including asymmetric three-dimensional effects. *J. Fluid Mech.* **577**, 105–126.

LELE, S. K. 1994 Compressibility effects in turbulence. *Annu. Rev. Fluid Mech.* **26**, 211–254.

LIEPMANN, H. W. & LAUFER, J. 1947 Investigations of free turbulent mixing. *NACA Tech. Note* 1257.

LIU, X. & KATZ, J. 2013 Vortex-corner interactions in a cavity shear layer elucidated by time-resolved measurements of the pressure field. *J. Fluid Mech.* **728**, 417–457.

MALONE, J., DEBIASI, M., LITTLE, J. & SAMIMY, M. 2009 Analysis of the spectral relationships of cavity tones in subsonic resonant cavity flows. *Phys. Fluids* **21** (5), 055103.

MAULL, D. J. & EAST, L. F. 1963 Three-dimensional flow in cavities. *J. Fluid Mech.* **16**, 620–632.

MORRIS, P. J. & GIRIDHARAN, M. G. 1991 The effect of walls on instability waves in supersonic shear layers. *Phys. Fluids* A **3** (2), 356–358.

MURRAY, N., SALLSTROM, E. & UKEILEY, L. 2009 Properties of subsonic open cavity flow fields. *Phys. Fluids* **21** (9), 095103.

MURRAY, R. C. & ELLIOTT, G. S. 2001 Characteristics of the compressible shear layer over a cavity. *AIAA J.* **39** (5), 846–856.

OHMICHI, Y. & SUZUKI, K. 2014 Flow structures and heating augmentation around finite-width cavity in hypersonic flow. *AIAA J.* **52** (8), 1624–1631.

OLSEN, M. G. & DUTTON, J. C. 2003 Planar velocity measurements in a weakly compressible mixing layer. *J. Fluid Mech.* **486**, 51–77.

PAPAMOSCHOU, D. & ROSHKO, A. 1988 The compressible turbulent shear layer: an experimental study. *J. Fluid Mech.* **197**, 453–477.

PLUMBLEE, H. E., GIBSON, J. S. & LASSITER, L. W. 1962 A theoretical and experimental investigation of the acoustical response of cavities in aerodynamic flow. *WADD TR*-61-75.

RAGAB, S. A. & WU, J. L. 1989 Linear instabilities in two-dimensional compressible mixing layers. *Phys. Fluids* A **1** (6), 957–966.

ROBINET, J.-C., DUSSAUGE, J.-P. & CASALIS, G. 2001 Wall effect on the convective-absolute boundary for the compressible shear layer. *Theor. Comput. Fluid Dyn.* **15** (3), 143–163.

ROCKWELL, D. & KNISELY, C. 1979 The organized nature of flow impingement upon a corner. *J. Fluid Mech.* **93** (3), 413–432.

ROCKWELL, D. & KNISELY, C. 1980 Observations of the three-dimensional nature of unstable flow past a cavity. *Phys. Fluids* **23** (3), 425–431.

ROSSITER, J. E. 1964 Wind-tunnel experiments on the flow over rectangular cavities at subsonic and transonic speeds. *Aeronautical Research Council Rep.* 3438.

ROSSMANN, T., MUNGAL, M. G. & HANSON, R. K. 2002 Evolution and growth of large-scale structures in high compressibility mixing layers. *J. Turbul.* **3** (1), 9.

https://doi.org/10.1017/jfm.2016.540 Published online by Cambridge University Press

ROWLEY, C. W., COLONIUS, T. & BASU, A. J. 2002 On self-sustained oscillations in two-dimensional compressible flow over rectangular cavities. *J. Fluid Mech.* **455**, 315–346.

SAMIMY, M. & ELLIOTT, G. S. 1990 Effects of compressibility on the characteristics of free shear layers. *AIAA J.* **28** (3), 439–445.

SAMIMY, M., REEDER, M. F. & ELLIOTT, G. S. 1992 Compressibility effects on large structures in free shear flows. *Phys. Fluids* A **4** (6), 1251–1258.

SANDHAM, N. D. & REYNOLDS, W. C. 1991 Three-dimensional simulations of large eddies in the compressible mixing layer. *J. Fluid Mech.* **224**, 133–158.

SAROHIA, V. 1977 Experimental investigation of oscillations in flows over shallow cavities. *AIAA J.* **15** (7), 984–991.

SIRIEIX, M. & SOLIGNAC, J. L. 1968 Contribution à l'étude experimental de la couche de mélange turbulente isobare d'un écoulement supersonique. In *Symposium on Separated Flows*, AGARD CP-4(1), pp. 241–270.

SLESSOR, M. D., ZHUANG, M. & DIMOTAKIS, P. E. 2000 Turbulent shear-layer mixing: growth-rate compressibility scaling. *J. Fluid Mech.* **414**, 35–45.

SMITS, A. J. & DUSSAUGE, J.-P. 2006 *Turbulent Shear Layers in Supersonic Flow*, 2nd edn. pp. 139–178. Springer.

STALLINGS, R. L. & WILCOX, F. J. 1987 Experimental cavity pressure distributions at supersonic speeds. *NASA Tech. Paper* 2683.

TAYLOR, J. R. 1997 *An Introduction to Error Analysis*, 2nd edn. pp. 140–141. University Science Books.

THEOFILIS, V. 2003 Advances in global linear instability analysis of nonparallel and three-dimensional flows. *Prog. Aerosp. Sci.* **39** (4), 249–315.

TRACY, M. B. & PLENTOVICH, E. B. 1997 Cavity unsteady-pressure measurements at subsonic and transonic speeds. *NASA Tech. Paper* 3669.

UKEILEY, L. & MURRAY, N. 2005 Velocity and surface pressure measurements in an open cavity. *Exp. Fluids* **38** (5), 656–671.

UNALMIS, O. H., CLEMENS, N. T. & DOLLING, D. S. 2004 Cavity oscillation mechanisms in high-speed flows. *AIAA J.* **42** (10), 2035–2041.

URBAN, W. D. & MUNGAL, M. G. 2001 Planar velocity measurements in compressible mixing layers. *J. Fluid Mech.* **431**, 189–222.

DE VICENTE, J., BASLEY, J., MESEGUER-GARRIDO, F., SORIA, J. & THEOFILIS, V. 2014 Three-dimensional instabilities over a rectangular open cavity: from linear stability analysis to experimentation. *J. Fluid Mech.* **748**, 189–220.

WAGNER, R. D. 1973 Mean flow and turbulence measurements in a Mach 5 free shear layer. *NASA Tech. Note* D-7366.

WAGNER, J. L., CASPER, K. M., BERESH, S. J., HENFLING, J. F., SPILLERS, R. W. & PRUETT, B. O. M. 2015*a* Mitigation of wind tunnel wall interactions in subsonic cavity flows. *Exp. Fluids* **56** (3), 59.

WAGNER, J. L., CASPER, K. M., BERESH, S. J., HUNTER, P. S., HENFLING, J. F., SPILLERS, R. W. & PRUETT, B. O. M. 2015*b* Fluid-structure interactions in compressible cavity flows. *Phys. Fluids* **27** (6), 066102.

WYGNANSKI, I. & FIEDLER, H. E. 1970 The two-dimensional mixing region. *J. Fluid Mech.* **41** (2), 327–361.

ZHANG, K. & NAGUIB, A. M. 2011 Effect of finite cavity width on flow oscillation in a low-Mach-number cavity flow. *Exp. Fluids* **51** (5), 1209–1229.

ZHANG, X. & EDWARDS, J. A. 1990 An investigation of supersonic oscillatory cavity flows driven by thick shear layers. *Aeronaut. J.* **94** (940), 355–364.

ZHUANG, N., ALVI, F. S., ALKISLAR, M. B. & SHIH, C. 2003 Aeroacoustics properties of supersonic cavity flows and their control. *AIAA Paper* 2003-3101.

ZHUANG, N., ALVI, F. S., ALKISLAR, M. B. & SHIH, C. 2006 Supersonic cavity flows and their control. *AIAA J.* **44** (9), 2118–2128.

ZHUANG, M., DIMOTAKIS, P. E. & KUBOTA, T. 1990 The effect of walls on a spatially growing supersonic shear layer. *Phys. Fluids* A **2** (4), 599–604.

https://doi.org/10.1017/jfm.2016.540 Published online by Cambridge University Press